UNIVERSIDADE DE SÃO PAULO
INSTITUTO DE FÍSICA DE SÃO CARLOS

Lucas Garcia Borges

Dynamics of matter waves undergoing Bloch oscillations in a ring cavity

São Carlos

2021

Lucas Garcia Borges

Dynamics of matter waves undergoing Bloch oscillations in a ring cavity

Dissertation presented to the Graduate Program in Physics at the Instituto de Física de São Carlos da Universidade de São Paulo, to obtain the degree of Master in Science.

Concentration area: Theoretical and Experimental Physics

Advisor: Prof. Dr. Romain Pierre Marcel Bachelard

Corrected version
(Original version available on the Program Unit)

São Carlos
2021

Borges, Lucas
Dynamics of matter waves undergoing Bloch oscillations in a ring cavity / Lucas Borges; advisor Romain Bachelard - corrected version -- São Carlos 2021.
68 p.

Dissertation (Master's degree - Graduate Program in Theoretical and Experimental Physics) -- Instituto de Física de São Carlos, Universidade de São Paulo - Brasil , 2021.

1. Bloch oscillations. 2. CARL. 3. EIT. 4. Three-level atoms. I. Bachelard, Romain, advisor. II. Title.

Primeiramente agradeço aos meus pais, Girceley e Carlos H., e a minha irmã, Maria Rita, pelo apoio incondicional em todos os momentos da minha trajetória acadêmica, apesar de não entenderem bem o que faço. Espero ser sempre capaz de retribuir esse apoio. Este trabalho todo é dedicado a eles.

Quero dedicar também esta monografia ao meu orientador, prof. Romain Bachelard, cuja dedicação e colaboração tornaram possível a construção deste trabalho. Tenho muita sorte de ter tido a oportunidade de trabalhar e aprender com ele, e ainda mais de conhecê-lo melhor pessoalmente. Agradeço também a todos os professores que me lecionaram durante esses 6 anos, em especial aos professores Philippe Courteille e Raul Celistrino, cujo empenho e dedicação mantém um exímio grupo de pesquisa, e ao professor Raphael Santarelli, meu primeiro orientador durante minha graduação.

Meu mestrado também não seria possível sem o apoio de todos os amigos que fiz ao longo desta jornada. Agradeço especialmente aos meus amigos de laboratório: Dalila Rivero, Marcia Frometa e Pablo Dias, cujas presenças foram essênciais para tornar essa minha jornada ao longo do mestrado inesquecível, e por acolherem um teórico no meio de tantos experimentais. Também não posso me esquecer dos amigos que estiveram comigo desde o começo da minha graduação, em especial: Aline Chan, que sempre me acolheu e me serviu a melhor comida de SanCa, te agradeço pessoalmente quando for me visitar; Lucas Oliveira, cuja presença sempre anima nossos grupos e nunca se esquece de uma data especial, obrigado por ser o melhor rommmate que tive; Vinicius Rossi, que apesar de sempre estarmos longe e minha constante demanda de atenção, isso nunca abalou nossa relação.

E a todas as outras pessoas que tive a sorte de encontrar ao longo desse caminho, muito obrigado por todos esses momentos, tristes ou felizes, que tivemos e ainda teremos!

ACKNOWLEDGEMENTS

I wish to thank the Instituto de Física de São Carlos for the support.

I would like to express my great gratitude to Prof. Romain Bachelard for his supervision and fellowship. And Prof. Philippe Courteille for welcoming me into his group.

This study was financed in part by the Coordenação de Aperfeiçoamento de Pessoal de Nível Superior – Brasil (CAPES) – Finance Code 001.

"It is good to have an end to journey toward;
but it is the journey that matters, in the end."
— Ursula K. Le Guin

ABSTRACT

BORGES, L. **Dynamics of matter waves undergoing Bloch oscillations in a ring cavity**. 2021. 68p. Dissertation (Master in Science) - Instituto de Física de São Carlos, Universidade de São Paulo, São Carlos, 2021.

The work developed in this thesis investigate the dynamics of ultracold atoms trapped in a ring cavity and undergoing Bloch oscillations due to the influence of a one-dimensional vertical optical lattice and of the gravitational force. In this configuration, the atoms collectively scatter light from the pump into the copropagating cavity mode, which then leads to a self-consistent grating of the matter: this mechanism was coined collective atomic recoil lasing (CARL). Such interaction between atomic motion and cavity modes provides a possible continuous and non-destructive method to monitor the Bloch oscillations dynamics, which could be implemented in atomic gravimeters. This dissertation investigates the fundamental problem of dissipation effects due to spontaneous emission of the atoms, which is responsible for a suppression of the Bloch oscillations signatures on the light modes. We also study a possible solution for this issue by including a third atomic level in the configuration to explore a probable dissipation reduction due to the phenomenon of electromagnetically induced transparency (EIT).

Keywords: Bloch oscillations. CARL. EIT. Gravimetry. Three-level atom.

RESUMO

BORGES, L. **Dinâmica de ondas de matéria realizando oscilações de Bloch em uma cavidade anelar**. 2021. 68p. Dissertação (Mestre em Ciências) - Instituto de Física de São Carlos, Universidade de São Paulo, São Carlos, 2021.

O trabalho desenvolvido nesta tese investiga a dinâmica de átomos ultra-frios aprisionados em uma cavidade anular e submetidos a oscilações de Bloch devido à influência de uma rede ótica vertical unidimensional e da força gravitacional. Nesta configuração, os átomos dispersam coletivamente a luz de pump para o modo copropagante da cavidade, o que então leva a uma organização autoconsistente da matéria: este mecanismo foi cunhado de recoil lasing atômico coletivo (CARL). Tal interação entre os modos de movimento atômico e cavidade proporciona um possível método contínuo e não destrutivo para monitorar a dinâmica das oscilações de Bloch, que poderia ser implementado em gravimetria atômica. Esta dissertação investiga o problema fundamental dos efeitos de dissipação devido à emissão espontânea dos átomos, que é responsável pela supressão das assinaturas das oscilações de Bloch nos modos de luz. Também estudamos uma possível solução para esta questão, incluindo um terceiro nível atômico na configuração para explorar uma provável redução da dissipação devido ao fenômeno da transparência induzida eletromagneticamente (EIT).

Palavras-chave: Oscilações de Bloch. CARL. EIT. Gravimetria. Átomos de três níveis.

LIST OF FIGURES

CONTENTS

1 INTRODUCTION

The measurement of the gravitational field is an important objective in the fields of geophysics, metrology, and many others as it provides informations of the planet's morphology and on the composition of the underground. In particular, a precise measure of the local gravity acceleration can have a strong impact on oil exploration, considering it could completely replace invasive methods, which are very costly. Since the last century, gravimetry has evolved from pendulums, springs, torsion balances and superconducting levitation instruments[1] until recently, to cold atom interferometry.[2] The latter takes advantage of an oscillatory phenomenon known as the atomic Bloch oscillations.

The phenomenon of Bloch oscillations was predicted theoretically by Felix Bloch in 1929[3] in a study of electrons in a periodic crystal potential, where it had been demonstrated that the application of a constant force on the confined electrons produces an oscillatory behavior instead of a uniform movement. Back in the 90's, the same phenomenon was demonstrated in cold atoms trapped in optical lattices when an external force was applied,[4] thus the name atomic Bloch oscillations.

The oscillations of the matter-waves due to the conservative potential provide a direct signature of the force, hence the potential for gravimetry. This was recently shown by the first measurements of gravity by that means,[2,5–7] reaching precisions of 10^{-7}. This makes Bloch oscillations a useful tool with a wide range of applications, e.g., oil prospection and metrology. However, experiments up to date have the disadvantage of relying on destructive measurements of the instantaneous velocity of the atoms, such as absorption imaging, which shatters the atomic cloud so a new ensemble is required to continue the oscillations measure. Consequently, thousands of realizations must be performed in order to produce a precise measurement of the force field, which in turn is spoiled by fluctuations in the cloud preparation, and requires more time for the integration.

To tackle the problem of destructive measurements, one possible solution is to combine the collective atomic effect of CARL (collective atomic recoil lasing), together with the Bloch oscillations, using the particularities of a ring cavity, as proposed by the project collaborators.[8–10] As the counterpropagating modes of the ring cavity have independent photon numbers, it allows a continuous harness of the light pulses resulting from the Bloch oscillations. This continuous measurement depends on a single realization, eliminating problems of fluctuations between realizations and drastically reducing the integration time. Consequently, the construction of an experiment to provide the first non-destructive measurement of Bloch oscillations by cold atoms was initiated in São Carlos, Brazil, with the support of the São Paulo Research Foundation (FAPESP), the Brazilian National Council for Scientific and Technological Development (CNPq) and the Coordination for

the Improvement of Higher Education Personnel (CAPES).

This project aims to continue the theoretical investigations of the continuous monitoring of Bloch oscillations in vertical ring cavities. Although a proof of principle has recently been proposed,[8] there are still caveats regarding dissipative effects, whose effect on the synchronization of oscillations has not been studied. The research of this thesis arises from the idea of including an additional atomic level in the used model of a two-level atom, to make use of the EIT (electromagnetic induced transparency) effect: this allows one to tune the optical characteristics of the atomic ensemble and reduce dissipative forces that arise from the light-matter interaction.

In the following sections, we present a brief review of the Bloch oscillations and CARL phenomena.

1.1 Bloch Oscillations

As mentioned earlier, Bloch oscillations were predicted since the first half of last century, but their observation in electrons is very challenging, mostly because of the scattering events by the lattice defects or impurities in natural crystals. On the other hand, in optical systems the relative absence of defects in optical lattice provides an excellent platform to observe such phenomenon.

To observe the Bloch oscillations with an atomic matter wave, we can consider two counterpropagating laser fields modes of equal intensity, with wave-number k, which produce a one-dimensional stationary wave (the optical lattice). The dynamics occurs in the presence of an homogeneous and constant force, which in our case is the gravitational force. We can write the Schroedinger equation to describe the time evolution of a single atom wave-function in the presence of the force and of an optical lattice:

$$i\hbar\frac{\partial}{\partial t}\psi(x,t) = (\mathcal{H} - \hat{V}_g(x))\psi(x,t), \tag{1.1.1}$$

where we have defined the gravitational potential $\hat{V}_g = mg\hat{x}$, and the one-dimensional Hamiltonian $\mathcal{H}$ composed of the atom kinetic energy and the optical lattice potential:

$$\mathcal{H} = \frac{\hat{p}^2}{2m} + V_o\cos^2(k\hat{z}), \tag{1.1.2}$$

with the atomic mass m, the gravitational acceleration g and V_o the optical lattice strength. From the Bloch oscillations theory[11],[12] we define the eigenfunctions $\varphi_{n,q}(x)$ of $\mathcal{H}$ as

$$\varphi_{n,q}(x) = e^{iqx}U_{n,q}(x), \tag{1.1.3}$$

which depends on the position x, the band index n and the quasimomentum q, restricted to the first Brillouin zone: $-k \leq q \leq k$. The periodic function $U_{n,q}(x) = U_{n,q}(x + \pi/k)$ has the same periodicity as the optical lattice and satisfy the Schroedinger equation

$$\left[\frac{(\hat{p} + \hbar q)^2}{2m} + V_o\cos^2(k\hat{z})\right]U_{n,q}(x) = \varepsilon_{n,q}U_{n,q}(x), \tag{1.1.4}$$

where $\varepsilon_{n,q}$ are the eigenvalues of $\mathcal{H}$, and periodic functions of the quasimomentum q with period $2k$. The action of the external force $F = mg$ on the system dynamics is incorporated in the wavefunction by performing a transformation of ψ to the accelerated frame:

$$\psi(x,t) = e^{iFxt/\hbar}\tilde{\psi}(x,t), \tag{1.1.5}$$

then, equation (1.1.1) becomes

$$i\hbar\frac{\partial}{\partial t}\tilde{\psi}(x,t) = \left[\frac{(\hat{p}+Ft)^2}{2m} + V_o\cos^2(k\hat{z})\right]\tilde{\psi}(x,t). \tag{1.1.6}$$

Comparing equation (1.1.6) to (1.1.4), we observe that the quasimomentum evolves in the presence of the applied external force F according to

$$q(t) = q(0) + \frac{Ft}{\hbar}. \tag{1.1.7}$$

The phenomenon of Bloch oscillations can be understood in terms of the quasimomentum q illustrated in the reduced-zone scheme of Fig. 1. When $q(t)$ reaches the edge of the Brillouin zone at $\pi/d = k$, it is reflected to the point $q = -\pi/d$, which corresponds to an oscillatory behavior in momentum space. After one Bloch period ($\tau_B = hF/d$), the quasimomentum fully spans the first Brillouin zone and returns to the same starting value of $q(0)$. Since the external force induces a uniform motion in quasimomentum space, the wave function $\tilde{\psi}$ is also periodic in time with period τ_B, which corresponds to oscillations in real space. In the case of the gravitational force, given by $F_g = mgx$, where g is the gravity acceleration, the Bloch oscillations frequency is $\nu_B = mg/2\hbar k$.

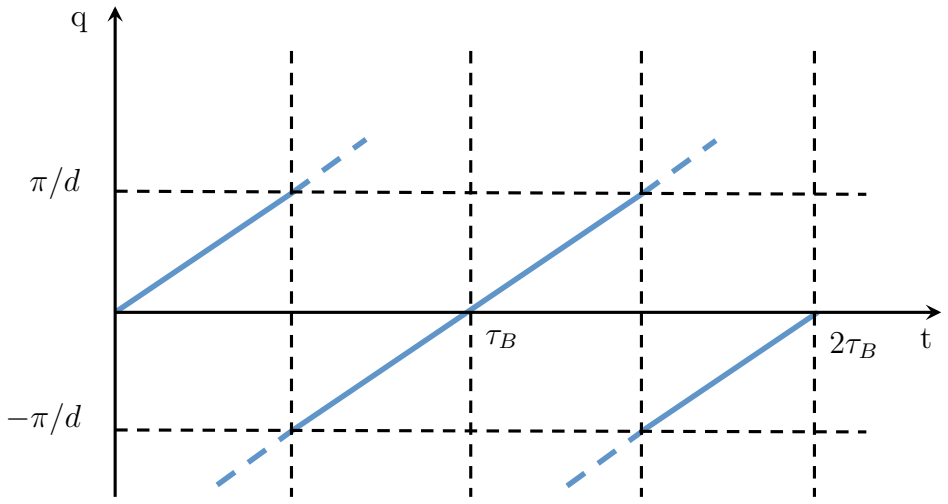

Figure 1 – Time-dependent quasimomentum $q(t)$ in the first Brillouin zone $\pi/d \leq q \leq \pi/d$.
Source: Adapted from SAMOYLOVA.[10]

In Fig. 2 we present the results of a recent experimental observation of Bloch oscillations of weakly-interacting bosonic Strontium atoms in a vertical optical lattice

under the action of the gravitational potential.[5] Each image shows a different realization of the experiment, since the time-of-flight method to measure the atoms momentum destroys the cloud, and a new ensemble had to be prepared to continue the experiment.

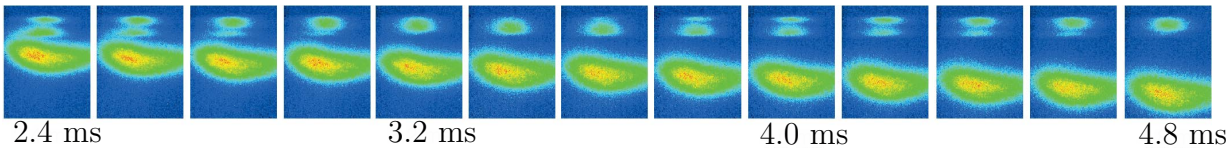

Figure 2 – Time-of-flight images of the atoms recorded for different times of evolution in the optical lattice potential. In the upper part of each frame, the atoms confined in the optical lattice perform Bloch oscillations for the combined effect of the periodic and gravitational potential. In the lower part, untrapped atoms fall down freely under the effect of gravity.
Source: Adapted from FERRARI.[5]

1.2 Collective Atomic Recoil Lasing

The collective atomic recoil laser (CARL) consists of the coherent amplification of the scattered light from an atomic cloud interacting with a counterpropagating laser beam. It was first predicted[13] as an atomic analogue of the free-electron laser (FEL), since it converts atomic momentum into coherent radiation.

The concept involves a monochromatic homogeneous beam of two-level atoms moving at the same velocity and a strong counterpropagating pump laser beam, which is Bragg-scattered by the atomic density defects. The interference between pump and scattered light then produces an optical potential, which in turns increases the density grating in a self-amplifying mechanism. Therefore, the CARL converts kinetic energy into coherent radiation, increasing the energy difference between probe and pump mediated by atomic bunching. The collective action of the atoms is depicted in Fig. 3.

The feedback of a single atom on the phase of the standing light wave is very weak, thus it is necessary to have many atoms moving collectively, and the phase of the standing wave needs to be not fixed. To satisfy these conditions, a ring cavity can be used, since the phase of the standing wave is not fixed by boundary conditions of the mirror surfaces; this is the motive why the first experimental realization of CARL used a ring cavity.[15] Furthermore, the counterpropagating fields in a ring cavity form separate modes carrying independent numbers of photons, which allows to measure independently their photon population. In addition the atoms self-arrange as they are trapped by the dipolar forces in the antinodes of the stationary wave, which then allows for the observation of the atomic movement backaction using the phase of the standing wave.

Considering that the pump mode intensity $|\alpha_p|^2$ is constant into the cavity, we aim at monitoring the evolution of the probe mode α, where $|\alpha_p|^2$ is the photon number. The coupling between the modes only happens in the presence of atoms due to backscattering

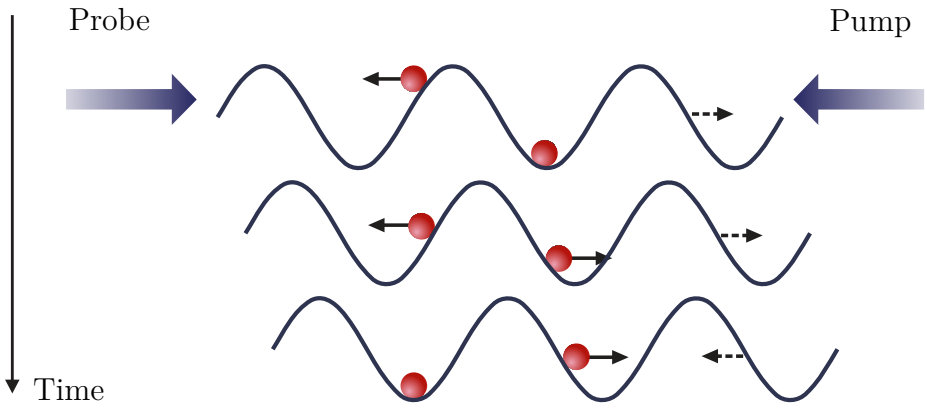

Figure 3 – The atom on the left is initially placed on the slope of the stationary wave. When accelerated towards the bottom of the potential, it pushes the wave to the right, so that the atom initially positioned in the valley of the potential is then granted potential energy and begins to oscillate.
Source: Adapted from COURTEILLE.[14]

events and is given by the single-photon light shift $U_o = \Omega_p/\Delta$, given by the rate between the single-photon Rabi frequency and the detuning from the atomic resonance, respectively. We can write the mode rate equation for α as[15]

$$\dot{\alpha} = -\kappa\alpha + iNU_o\alpha_p \sum_j e^{2ikx_j}, \tag{1.2.1}$$

where κ is the cavity decay, which describes the photon loss through the cavity mirror, k is the light modes wavenumber, x_j is the j-th atom position and N the number of atoms. The second term in the above expression is the photon gain of the probe from the pump mode through backscattering. The atom at position x_j feels the classical potential of the stationary light wave as the dipolar force, then the dynamics of the atom through the scattering process is given by this force in the far detuned regime[15]

$$m\ddot{x}_j = -2i\hbar kU_o(\alpha_p\alpha^* e^{ikx_j} - \alpha_p^*\alpha e^{-ikx_j}). \tag{1.2.2}$$

1.3 Proposed set-up

The setup investigated in this thesis consists of a cloud of ultracold atoms confined in a vertical optical standing wave, as depicted in Fig. 4, where it is possible to combine both effects of Bloch oscillations and the CARL. The optical lattice, with the lattice constant π/k_l, is generated by two external laser beams detuned sufficiently far from the atomic resonance and intersecting at the location of the atoms under the angle β defined by $K\sin(\beta/2) = k_l$, where K is the wavenumber of the laser beams.[10] This externally imposed optical lattice traps the atoms in a one-dimensional potential $\hbar W_o \sin(2kz)$ along the $\hat{\mathbf{z}}$ axis, where the potential depth is denoted by $\hbar W_o$. In addition, the atoms are also exposed to the gravitational potential $m_o gz$, where m_o is the atomic mass and g is the

gravitational acceleration. As a result, the atoms undergo Bloch oscillations with frequency $\nu_b = mg/2\hbar k^4$ under the influence of the applied gravitational force.

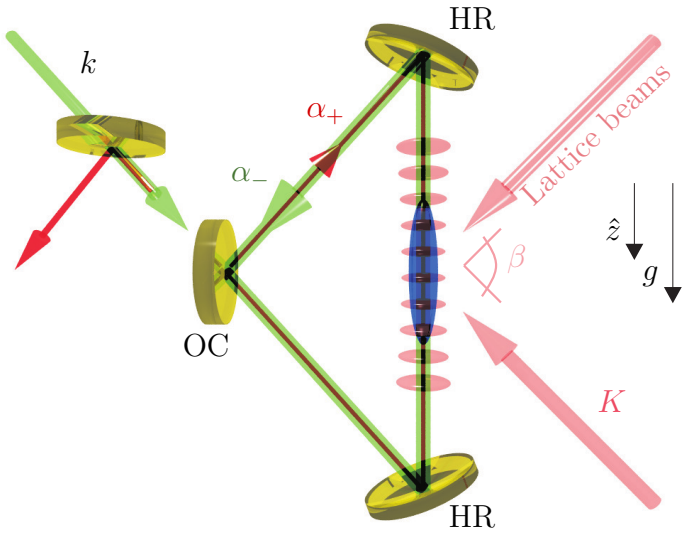

Figure 4 – Scheme of a ring cavity consisting of two high-reflecting mirrors (HR) and one output coupler (OC) interacting with an ultra-cold atoms cloud stored in one arm of the ring cavity. The cavity modes are the pump and probe modes (α_+ and α_- respectively). Two lasers (K) crossing the cavity mode at the location of the cloud under angles $\beta/2$ generate an optical lattice whose periodicity is commensurate with the standing wave created by the pump and probe modes. The atoms are also subject to an external accelerating force $m_o g$.
Source: Adapted from SAMOYLOVA.[10]

In Chapter 2, we derive the Bloch equations for a multi-level atom system, using the master equation approach since we are interested in describing the dissipation effects of spontaneous emission in our system. The general equations are used in following Chapters 3 and 4, where they are adapted to the two- and three-level atoms, respectively. We also perform an analysis of the stationary solutions, optical forces and the light field dynamics for those systems.

We describe the EIT effect using the three-level atom equations in chapter 5. Then we show the impact of the third level on the optical forces and the radiative pressure force reduction that can be generated.

The Bloch oscillations in both two- and three-level atoms are derived in Chapter 6, where we use a momentum expansion for the atomic wave-function. First we reproduce results for the 2LA adiabatic elimination case, studied in previous works. Then, we derive the von Neumann equation for the three-level system to observe the dissipations effects and the third level impact on the Bloch oscillations.

2 MANY-ATOM OPTICAL BLOCH EQUATIONS

To obtain the equations that describe the CARL dynamics, we must first derive the equations for the internal degrees of freedom of the atoms. To solve this problem, we could use the Schroedinger equation and describe the temporal evolution of the state of the system. However, within this formalism, we cannot describe the dissipative process of spontaneous emission as the atom is led to an overlap of many states of momentum and has to be described by a distribution of wave functions.

To calculate the probability of finding the system within this distribution, we use the formalism of the density matrix operators that describes a statistical mixture of quantum states. The equations that describe the temporal evolution of the elements of the density matrix of an atom in a field are the optical Bloch equations[16] (not related to the Bloch oscillations, although named after the same person). The following derivation aims to introduce the notation and terminology used throughout this thesis and establish the dynamical equations for the next chapters.

2.1 Density matrix

Let us consider some atoms trapped in an optical cavity. We call Ψ the atomic wave-function, whose discrete states of quantized degrees of freedom can be described by those eigenfunctions ψ_j of the unperturbed Hamiltonian operator $\mathcal{H}_o$. The Hamiltonian eigenvalues define the set of energy levels E_j given by $\hbar\omega_j$ related by

$$\mathcal{H}_o \left|\psi_j\right\rangle = \hbar\omega_j \left|\psi_j\right\rangle, \tag{2.1.1}$$

$$\langle \mathbf{r}|\psi_j\rangle = \psi_j(\mathbf{r}), \tag{2.1.2}$$

where $j \in \mathbb{N}$. The eigenstates ψ_j form a complete orthonormal basis

$$\int \psi_j^* \psi_k \mathrm{d}\vec{\mathbf{r}} = \delta_{jk}, \tag{2.1.3}$$

with δ_{jk} being the Dirac delta function. The atomic wave-function $\Psi(\mathbf{r}, t)$ satisfies the Schrödinger equation

$$i\hbar\frac{\partial\Psi}{\partial t} = \mathcal{H}\Psi, \tag{2.1.4}$$

where $\mathcal{H}$ is the system Hamiltonian, composed of the Hamiltonians of the unperturbed atom ($\mathcal{H}_o$), the light field ($\mathcal{H}_{field}$) and the interaction between them ($\mathcal{H}_{int}$):

$$\mathcal{H} = \mathcal{H}_o + \mathcal{H}_{field} + \mathcal{H}_{int}. \tag{2.1.5}$$

The unperturbed, or atomic Hamiltonian can be written as the sum of the kinetic energy and the N_l atomic levels $|\psi_j\rangle$ energies

$$\mathcal{H}_o = -\frac{\hbar^2}{2m_o}\nabla^2 + \sum_{j=1}^{N_l} \hbar\omega_j \left|\psi_j\right\rangle\!\left\langle\psi_j\right|, \tag{2.1.6}$$

where m_o is the atomic mass.

The atoms are driven by a near-resonance monochromatic laser, with frequency slightly detuned from the atomic resonance, which allows the particles to absorb the incoming photons and transition between energy levels. We consider an electric field due to a monochromatic electromagnetic wave[17] which, at the atomic position $\mathbf{r}$, can be written as

$$\hat{\mathbf{E}}(r,t) = \frac{1}{2}\Big(\hat{\mathbf{E}}^{+}(\mathbf{r},t) + \hat{\mathbf{E}}^{-}(\mathbf{r},t)\Big), \tag{2.1.7}$$

$$\hat{\mathbf{E}}^{+}(\mathbf{r},t) = \mathcal{E}\hat{a}e^{i(\mathbf{k}\cdot\mathbf{r}-\tilde{\omega}t)}\hat{\mathbf{e}} = \hat{\mathbf{E}}^{-}(\mathbf{r},t)^{\dagger}. \tag{2.1.8}$$

$\hat{a}$ is the annihilation operator of the field mode, k is the field wave-vector and $\tilde{\omega}$ its frequency with $\mathcal{E} = i\Big(\frac{\hbar\tilde{\omega}}{2\epsilon_0 V}\Big)^{1/2}$, where V is the cavity volume. The Hamiltonian for this light field is given by

$$\mathcal{H}_{field} = \hbar\tilde{\omega}\hat{a}^{\dagger}\hat{a}. \tag{2.1.9}$$

We can solve equation (2.1.4) by the expansion of Ψ in the orthonormal basis of the N_l unperturbed atomic states $|\psi_j\rangle$

$$\left|\Psi(\mathbf{r},t)\right\rangle = \sum_{j=1}^{N_l} c_j(t)\left|\psi_j(\mathbf{r})\right\rangle, \tag{2.1.10}$$

$$\langle\psi_j(\mathbf{r})|\psi_j(\mathbf{r})\rangle = \delta_{jk}, \tag{2.1.11}$$

where c_j are the complex amplitudes. For the free-atom case, where $\mathcal{H} = \mathcal{H}_o$, we can see that its time dependence is given by

$$c_j(t) = c_j(0)e^{-i\omega_j t}. \tag{2.1.12}$$

Considering that the eigenstates in (2.1.2) form a orthonormal basis we can define the density matrix ρ

$$\hat{\rho} = \left|\Psi\right\rangle\!\left\langle\Psi\right|, \tag{2.1.13}$$

whose elements are given by

$$\hat{\rho} = \sum_{j,k} c_j^* c_k \hat{\rho}_{jk}. \tag{2.1.14}$$

We have here introduced

$$\hat{\rho}_{jk} = \left|\psi_j\right\rangle\!\left\langle\psi_k\right|, \tag{2.1.15}$$

$$\rho_{jk} = c_j^* c_k, \quad \rho_{jk}^* = \rho_{kj}, \tag{2.1.16}$$

with diagonal elements corresponding to energy levels occupations, populations, and off-diagonal elements being related to the coherences between different levels.

2.2 Dipole approximation

In the presence of the light field the electron cloud of the atom is distorted in the direction of the electric field, inducing an effective electric dipole in the system. The induced dipole oscillates and radiates electromagnetic waves as a classical oscillating dipole would, therefore modifying the electric field.[18] To derive the interaction Hamiltonian for the Bloch equations we begin by calculating the polarization vector, which is obtained from the sum of the dipole moments of each atom in the system

$$\mathbf{P} = \sum_i \hat{\mathbf{d}}_\mathbf{i} \delta(\mathbf{r} - \mathbf{r}_i). \tag{2.2.1}$$

We have here defined the induced-dipole moment operator $\hat{\mathbf{d}}_\mathbf{i}$ of the i-th atom as

$$\hat{\mathbf{d}}_\mathbf{i} = -e\hat{\mathbf{r}}, \tag{2.2.2}$$

$$\left\langle \hat{\mathbf{d}}_i \right\rangle = -e \left\langle \Psi_i \right| \hat{\mathbf{r}} \left| \Psi_i \right\rangle, \tag{2.2.3}$$

where e is the electron charge. Performing the wave-functions expansion (2.1.10) in the unperturbed states we get

$$\left\langle \hat{\mathbf{d}} \right\rangle = -e \sum_{j,k} \rho_{kj} \mathbf{p}_{jk}, \tag{2.2.4}$$

with the definition of the time-independent dipole matrix elements:

$$\mathbf{p}_{jk} = -e \left\langle \psi_j \right| \hat{\mathbf{r}} \left| \psi_k \right\rangle, \quad \mathbf{p}^*_{jk} = \mathbf{p}_{kj}. \tag{2.2.5}$$

In the presence of the external field the momentum part of the unperturbed Hamiltonian is modified into

$$\frac{\hbar^2 \nabla^2}{2m_o} \rightarrow \frac{1}{2m_o}[-i\hbar\boldsymbol{\nabla} + e\mathbf{A}(\mathbf{r},t)]^2 - e\Phi(\mathbf{r},t), \tag{2.2.6}$$

where $\mathbf{A}(\mathbf{r},t)$ and $\Phi(\mathbf{r},t)$ are respectively the vector and scalar potentials of the external field and $\hat{p}$ is the momentum operator in the atomic Hamiltonian (2.1.6). In the Coloumb gauge the vector potential satisfies the wave function

$$\nabla^2 \mathbf{A} - \frac{1}{c^2}\frac{\partial^2 \mathbf{A}}{\partial t^2} = 0, \tag{2.2.7}$$

with solution $\mathbf{A} = \mathbf{A}_0 e^{i\mathbf{kr} - i\omega_k t} - c.c.$, where $k = 2\pi/\lambda$ is the field wave-vector and λ its wavelength. Considering r comparable with typical atomic dimensions ($\sim$ Å), and optical wavelengths ($400 - 700nm$), one has $kr \ll 1$; hence over the extent of an atom the vector potential can be considered spatially uniform $\mathbf{A}(\mathbf{r},t) \simeq \mathbf{A}(t)$, which is referred as the "dipole approximation". In this gauge, and after a unitary transformation, equation (2.2.6) becomes

$$\frac{1}{2m_o}[-i\hbar\boldsymbol{\nabla} + e(\mathbf{A} + \boldsymbol{\nabla}\chi)]^2 - e\frac{\partial \chi}{\partial t}. \tag{2.2.8}$$

Choosing the gauge function $\chi(\mathbf{r},t) = -\mathbf{A}\cdot\mathbf{r}$, we obtain the following relations

$$\boldsymbol{\nabla}\chi = -\mathbf{A}, \tag{2.2.9}$$

$$\frac{\partial\chi}{\partial t} = -\mathbf{r}\cdot\frac{\partial\mathbf{A}}{\partial t} = -\mathbf{r}\cdot\mathbf{E}. \tag{2.2.10}$$

Considering the Hamiltonian in equation (2.1.5) we can identify the interaction Hamiltonian in the above equations as

$$\mathcal{H}_{int} = -\hat{\mathbf{d}}\cdot\mathbf{E}. \tag{2.2.11}$$

Although the interaction between atom and light in the dipole approximation considers a locally constant electric field, it is valid only over the atom size, and it changes with its position relative to the light field wave. Thus, since our system relies on momentum exchange between matter and light, it is still necessary to consider the spatial variation of $\hat{\mathbf{E}}$ through $e^{\pm ikr}$ in equation (2.1.8), which describes the atom momentum recoil due to an photon absorption/emission.

2.3 Rotating wave approximation

Considering the atomic dipole moment in the direction of the electric field, the atom-field interaction Hamiltonian becomes

$$\mathcal{H}_{int} = \tfrac{1}{2}\sum_{j,l}^{N_l}(\hat{\rho}_{lj}\hat{\mathbf{p}}_{jl} + \hat{\rho}_{jl}\hat{\mathbf{p}}_{lj})\Big(\hat{\mathbf{E}}^{+}(\mathbf{r})e^{-i\tilde{\omega}t} + \hat{\mathbf{E}}^{-}(\mathbf{r})e^{i\tilde{\omega}t}\Big). \tag{2.3.1}$$

In the unperturbed case the density matrix elements ρ_{jl} evolves according to $\rho_{jl}(t) = \rho_{jl}(0)e^{-i\omega_{jl}t}$, where $\omega_{jl} = \omega_j - \omega_l$, thus the products $\rho_{jl}\hat{\mathbf{E}}^{+}e^{-i\tilde{\omega}t}$ and $\rho_{lj}\hat{\mathbf{E}}^{-}e^{i\tilde{\omega}t}$ rotate much faster than the optical frequency, for a positive ω_{jl}. Hence we can neglect such terms performing the denominated rotating wave approximation (RWA).[19] One can also argue that these terms do not conserve energy (in first-order processes) since they can be interpreted as the absorption of a photon combined with the de-excitation of the atom, or with the emission of a photon combined with the excitation of the atom, respectively. Anyhow, the interaction Hamiltonian can then be approximated as

$$\mathcal{H}_{int}^{\mathrm{RWA}} = \frac{\hbar}{2}\sum_{j>l}^{N_l}(\Omega_{jl}\rho_{jl} + h.c.), \tag{2.3.2}$$

with the Rabi frequency defined as

$$\Omega_{jl} = \frac{\mathbf{p_{lj}}\cdot\hat{\mathbf{E}}^{+}(\mathbf{r})}{\hbar}. \tag{2.3.3}$$

2.4 Master equation

Let us now derive the dynamical equations for the density matrix elements considering the effect of spontaneous emission using the master equation formalism through the von Neumann equation for $\hat{\rho}$:

$$\dot{\hat{\rho}} = \frac{i}{\hbar}[\hat{\rho}, \mathcal{H}] + \mathcal{L}_d\hat{\rho}. \tag{2.4.1}$$

$\mathcal{H}$ is the total Hamiltonian (2.1.5) after the RWA, and $\mathcal{L}_d\hat{\rho}$ is the dissipative term, denominated the Lindblad superoperator[20]:

$$\mathcal{L}_d\hat{\rho} = \sum_{j,k} \gamma_{jk}(2\hat{\rho}_{kj}\hat{\rho}\hat{\rho}_{jk} - \hat{\rho}_{jk}\hat{\rho}_{kj}\hat{\rho} - \hat{\rho}\hat{\rho}_{jk}\hat{\rho}_{kj}), \tag{2.4.2}$$

with $\gamma_{jk} = \Gamma_{jk}/2$ the linewidth of the atomic levels transition of $|\psi_j\rangle$ to $|\psi_k\rangle$.

The density matrix elements derivatives can be derived as

$$\dot{\rho}_{jk} = \frac{i}{\hbar}\langle j|\,[\hat{\rho}, \mathcal{H}]\,|k\rangle + \langle j|\,\mathcal{L}_d\hat{\rho}\,|k\rangle\,, \tag{2.4.3}$$

which leads to the following expression for the coherent part:

$$\frac{i}{\hbar}\langle j|\,[\hat{\rho}, \mathcal{H}]\,|k\rangle = -i\omega_{jk}\rho_{jk} - \frac{i}{2}\sum_{l>m}^{N_l}(\Omega_{lm}\rho_{mk}\delta_{lj} + \Omega^*_{lm}\rho_{lk}\delta_{mj} - \Omega_{lm}\rho_{jl}\delta_{mk} - \Omega^*_{lm}\rho_{jm}\delta_{lk}), \tag{2.4.4}$$

where $\omega_{jk} = \omega_j - \omega_k$. For the dissipative part we have

$$\langle j|\,\mathcal{L}_d\hat{\rho}\,|k\rangle = \sum_l 2\gamma_{kl}\delta_{jk}\rho_{ll} - \sum_l(\gamma_{lj} + \gamma_{lk})\rho_{jk}. \tag{2.4.5}$$

Gathering the expressions above, we obtain the optical Bloch equations with the spontaneous emission, which describes the time evolution of the density matrix elements for a N_l-level atom system:

$$\begin{aligned}\frac{\mathrm{d}\rho_{jk}}{\mathrm{d}t} = 2\sum_l^{N_l}\gamma_{kl}\rho_{ll}\delta_{jk} - \left[\sum_l^{N_l}(\gamma_{lj} + \gamma_{lk}) + i\omega_{jk}\right]\rho_{jk} \\ + \frac{i}{2}\sum_{l>m}^{N_l}(\Omega_{lm}\rho_{mk}\delta_{lj} + \Omega^*_{lm}\rho_{lk}\delta_{mj} - \Omega_{lm}\rho_{jl}\delta_{mk} - \Omega^*_{lm}\rho_{jm}\delta_{lk}).\end{aligned} \tag{2.4.6}$$

3 TWO-LEVEL ATOMS

In this chapter we apply the definitions and equations made so far to the simple case of two-level atoms (2LA) excited by counterpropagating light fields. In this specific case we consider the derived Bloch equations in chapter 2 setting $N_l = 2$.

3.1 Bloch equations for two-level systems

We here consider a single atom with only two accessible energy levels denominated $|1\rangle$ and $|2\rangle$, respectively the non-degenerate ground and excited state. The electric field of the incident light field with two counter-propagating modes is given in the Heisenberg picture by

$$\hat{\mathbf{E}}(z,t) = \mathrm{Re}\left\{\mathcal{E}\left(\hat{a}_+ e^{ikz} + \hat{a}_- e^{-ikz}\right)e^{-i\tilde{\omega}t}\right\}\hat{\mathbf{e}}, \tag{3.1.1}$$

with

$$\mathcal{E} = i\left(\frac{\hbar\tilde{\omega}}{2\epsilon_0 V}\right)^{1/2}. \tag{3.1.2}$$

$\hat{a}_\pm$ are the annihilation operators of the field modes, which satisfy the commutation relations $\left[\hat{a}_\pm^\dagger, \hat{a}_\pm\right] = 1$ and $[\hat{a}_\pm, \hat{a}_\mp] = 0$, k is the wave-vector of the modes and $\tilde{\omega}$ their frequency. The field polarization is set in the same direction $\hat{\mathbf{e}}$ of the atomic dipole.

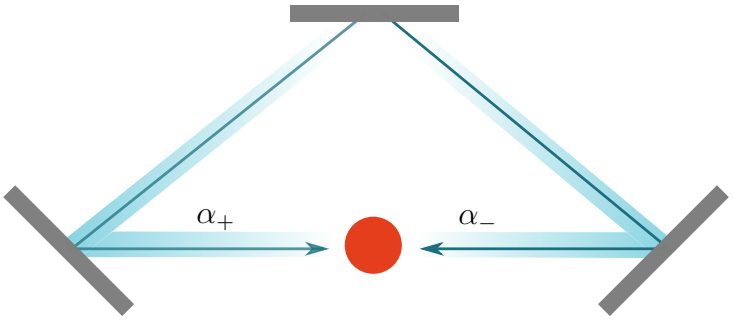

Figure 5 – Diagram of a atom (atomic cloud) excited by two counterpropagating light modes in a ring cavity.
Source: By the author.

With the electric field definition, the Hamiltonian in the rotating wave approximation for the 2LA writes

$$\mathcal{H} = -\frac{\hbar^2}{2m_o}\boldsymbol{\nabla}^2 - \hbar\Delta_{21}\,|2\rangle\langle 2| + \hbar\tilde{\omega}\hat{a}_\pm^\dagger\hat{a}_\pm + \hbar g_{21}\hat{a}_\pm^\dagger e^{\mp ikz}\,|1\rangle\langle 2| + h.c., \tag{3.1.3}$$

where $g_{21} = d_{12}\mathcal{E}/2\hbar$ is the light-atom coupling force.

Since there is no dipole element between the same levels ($\mathbf{p}_{jj} = 0$), from (2.2.4) the electric dipole moment for the 2LA reads

$$\left\langle \hat{\mathbf{d}} \right\rangle = -e(\rho_{12}\hat{\mathbf{p}}_{21} + \rho_{21}\hat{\mathbf{p}}_{12}), \tag{3.1.4}$$

$$= d_{12}(\rho_{12} + \rho_{21})\hat{\mathbf{e}}, \tag{3.1.5}$$

where we have introduced the electric dipole moment $d_{12}\,\hat{\mathbf{e}} = -e\mathbf{p}_{12} = -e\mathbf{p}_{21}$, given by

$$d_{12} = \sqrt{\frac{3\pi\epsilon_0\hbar\Gamma_{12}}{k^3}}, \tag{3.1.6}$$

and Ω_{21} the real Rabi frequency for this two-level system, defined as in equation (2.3.3)

$$\hbar\Omega_{21} = \left\langle \hat{\mathbf{d}} \cdot \hat{\mathbf{E}} \right\rangle, \tag{3.1.7}$$

$$\Omega_{21} = \frac{d_{12}\mathcal{E}}{\hbar}(\alpha_+ e^{ikz} + \alpha_- e^{-ikz}). \tag{3.1.8}$$

With those definitions, and after some algebra, we obtain the Bloch equations for the 2LA from the general expression in (2.4.6), which are given by the following set of ordinary differential equations

$$\frac{\mathrm{d}\rho_{11}}{\mathrm{d}t} = 2\gamma_2\rho_{22} + \frac{i}{2}(\Omega_{21}^*\rho_{21}e^{i\tilde{\omega}t} - \Omega_{21}\rho_{12}e^{-i\tilde{\omega}t}), \tag{3.1.9a}$$

$$\frac{\mathrm{d}\rho_{22}}{\mathrm{d}t} = -2\gamma_2\rho_{22} - \frac{i}{2}(\Omega_{21}^*\rho_{21}e^{i\tilde{\omega}t} - \Omega_{21}\rho_{12}e^{-i\tilde{\omega}t}), \tag{3.1.9b}$$

$$\frac{\mathrm{d}\rho_{12}}{\mathrm{d}t} = -(\gamma_{12} - i\omega_{21})\rho_{12} - \frac{i}{2}\Omega_{21}^*e^{i\tilde{\omega}t}(\rho_{11} - \rho_{22}), \tag{3.1.9c}$$

$$\frac{\mathrm{d}\rho_{21}}{\mathrm{d}t} = -(\gamma_{21} + i\omega_{21})\rho_{21} + \frac{i}{2}\Omega_{21}e^{-i\tilde{\omega}t}(\rho_{11} - \rho_{22}). \tag{3.1.9d}$$

Remark that it is necessary to add the term $\gamma_{21}\rho_{22}$ to the derivative of the first level population to satisfy the constraint of fixed total population:

$$\rho_{11} + \rho_{22} = 1.$$

3.2 Matrix representation

Let us now rewrite the Bloch equations into the frame of the driving field, by introducing the following variables, which correspond to the $|1\rangle$-$|2\rangle$ transition coherence:

$$\rho_{21} = \sigma_{21}e^{-i\tilde{\omega}t}. \tag{3.2.1}$$

Then equation (3.1.9d) becomes

$$\frac{\mathrm{d}}{\mathrm{d}t}\left(\sigma_{21}e^{-i\tilde{\omega}t}\right) = -(\gamma_{21} + i\omega_{21})\sigma_{21}e^{-i\tilde{\omega}t} + \frac{i}{2}\Omega_{21}e^{-i\tilde{\omega}t}(\rho_{11} - \rho_{22}), \tag{3.2.2}$$

$$\frac{\mathrm{d}\sigma_{21}}{\mathrm{d}t} = -(\gamma_{21} - i\Delta_{21})\sigma_{21} + \frac{i}{2}\Omega_{21}(\rho_{11} - \rho_{22}), \tag{3.2.3}$$

where $\Delta_{21} = \tilde{\omega} - \omega_{21}$ is the detuning between atomic resonance and the field frequency. Therefore we can write the Bloch equations system (3.2.4) in a matrix equation form

$$\frac{\mathrm{d}}{\mathrm{d}t}\begin{pmatrix}\rho_{11}\\ \rho_{22}\\ \sigma_{12}\\ \sigma_{21}\end{pmatrix} = \begin{pmatrix} 0 & \Gamma_{21} & -\frac{i}{2}\Omega_{21} & \frac{i}{2}\Omega_{21}^{*} \\ 0 & -\Gamma_{21} & \frac{i}{2}\Omega_{21} & -\frac{i}{2}\Omega_{21}^{*} \\ -\frac{i}{2}\Omega_{21}^{*} & \frac{i}{2}\Omega_{21}^{*} & -\Lambda_{21} & 0 \\ \frac{i}{2}\Omega_{21} & -\frac{i}{2}\Omega_{21} & 0 & -\Lambda_{21}^{*} \end{pmatrix}\begin{pmatrix}\rho_{11}\\ \rho_{22}\\ \sigma_{12}\\ \sigma_{21}\end{pmatrix}, \tag{3.2.4}$$

where $\Lambda_{21} = \gamma_{21} + i\Delta_{21}$ and $\Gamma_{21} = 2\gamma_{21}$.

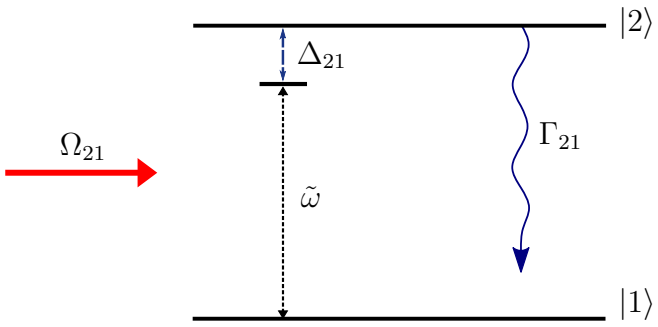

Figure 6 – Two-level energy diagram for an atom excited by a laser field Ω_{21}, where Δ_{21} is the detuning between the optical field frequency $\tilde{\omega}$ and the atomic levels transition, and Γ_{21} is the decay rate for the spontaneous emission of the excited level.

Source: By the author.

3.3 Reduced Bloch equations

For the two-level atom case, we can reduce the equations in (3.2.4) to a two-equation system by defining the populations difference $\mathcal{D} = \frac{1}{2}(\rho_{11} - \rho_{22})$, whose derivative is given by

$$\frac{\mathrm{d}\mathcal{D}}{\mathrm{d}t} = \frac{1}{2}\left(\frac{\mathrm{d}\rho_{11}}{\mathrm{d}t} - \frac{\mathrm{d}\rho_{22}}{\mathrm{d}t}\right), \tag{3.3.1}$$

$$= \gamma_{12}\rho_{22} + \frac{i}{2}(\Omega_{21}^{*}\sigma_{21} - \Omega_{21}\sigma_{12}), \tag{3.3.2}$$

$$= \Gamma_{21}\left(\frac{1}{2} - \mathcal{D}\right) + \frac{i}{2}(\Omega_{21}^{*}\sigma_{21} - \Omega_{21}\sigma_{12}). \tag{3.3.3}$$

Hence the Bloch equations for the 2LA can be simplified to the following coupled differential equations system

$$\frac{\mathrm{d}\sigma_{12}}{\mathrm{d}t} = -\Lambda_{21}\sigma_{12} - i\Omega_{21}^{*}\mathcal{D}, \tag{3.3.4a}$$

$$\frac{\mathrm{d}\mathcal{D}}{\mathrm{d}t} = \Gamma_{21}\left(\tfrac{1}{2} - \mathcal{D}\right) + \mathrm{Im}\{\sigma_{12}\Omega_{21}\}. \tag{3.3.4b}$$

We present the populations dynamics for the 2LA for different values of detuning in Fig. 7. At resonance ($\Delta_{21} = 0$), the atom periodically performs a full population inversion, which is reduced for a finite detuning.

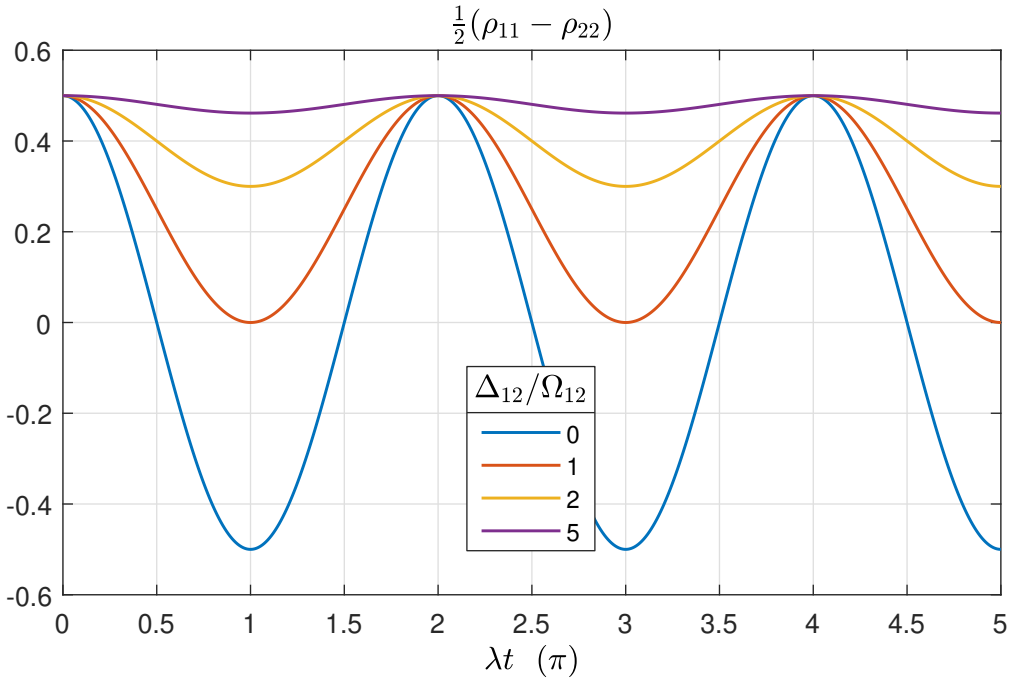

Figure 7 – Rabi oscillations for the populations difference $(\rho_{11}-\rho_{22})/2$ of a two-level atom with different values for the detuning where $\lambda = \sqrt{\Omega^2+\Delta^2}$.
Source: By the author.

3.4 Stationary case

Due to the spontaneous emission, the system reaches a steady-state which is described by the solution of equations (3.3.4), where the left-hand terms are set to zero. The stationary solutions for the coherence and the population difference are given by

$$\sigma_{12}(\infty) = -i\frac{\Omega_{21}^{*}\mathcal{D}}{\Lambda_{21}}, \tag{3.4.1}$$

$$\mathcal{D}(\infty) = \frac{1}{2} + \frac{\mathrm{Im}\{\sigma_{12}\Omega_{21}\}}{\Gamma_{21}}. \tag{3.4.2}$$

After some algebra we get

$$\sigma_{12}(\infty) = -i\Omega_{21}\frac{\Lambda_{21}^{*}}{|\Omega_{21}|^2+2|\Lambda_{21}|^2}, \tag{3.4.3}$$

$$\mathcal{D}(\infty) = \frac{1}{4}\frac{\Gamma_{21}^2+4\Delta_{21}^2}{|\Omega_{21}|^2+2|\Lambda_{21}|^2}. \tag{3.4.4}$$

In Fig. 8, one can observe the influence of the decay rate influence on the stationary state of the atomic level.

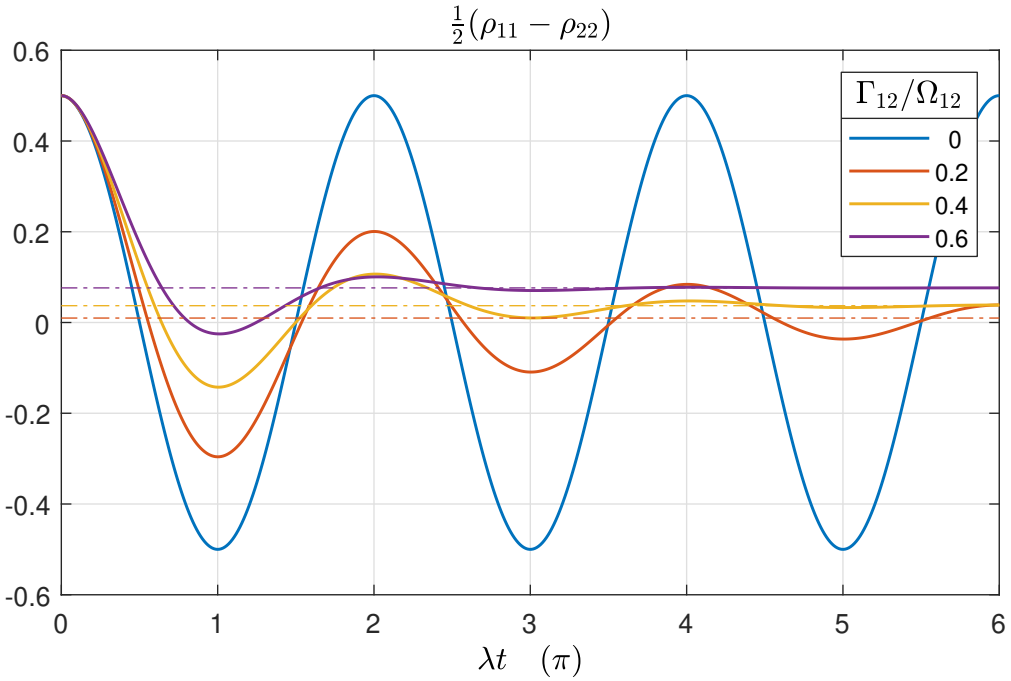

Figure 8 – Rabi oscillations of a two-level atom with spontaneous emission in the resonance regime ($\Delta_{21} = 0$). For increasing decay rate the population difference reaches a stationary value faster.

Source: By the author.

3.5 Optical fields

To account for the light fields dynamics in the ring cavity due to the feedback of the atomic dipoles on the light fields, we need to derive the dynamics of the photon annihilation and destruction operators through the Heisenberg equation. So far we neglected the position operator $\hat{z}$ present in the fields as the kick-operator $e^{ik\hat{z}}$, however it has a huge importance on the atomic external degrees of freedom dynamics. The light fields interacts with the atoms by driving transitions within its levels, and they exchange a momentum quantity of $\hbar k$ during the scattering.

However, for strong light intensities we may replace the quantum operators by complex numbers $\hat{z} \equiv z$, which is valid since the light field photon number is much greater than unity. From the system Hamiltonian (3.1.3), we can derive the derivatives of the field complex amplitudes through the Heisenberg equation

$$\frac{\mathrm{d}\hat{a}_\pm}{\mathrm{d}t} = \frac{i}{\hbar}[\mathcal{H}, \hat{a}_\pm], \tag{3.5.1}$$

$$= -ig\hat{\sigma}_{12}e^{\mp ik\hat{z}}. \tag{3.5.2}$$

Let us now include the losses and the pump of the fields. We first consider the cavity decay κ that stems from the finite reflectivity of the mirrors

$$\left.\frac{\partial\hat{a}_\pm}{\partial t}\right|_{decay} = -\kappa\hat{a}_\pm. \tag{3.5.3}$$

We also consider the field detuning from the cavity resonance frequency ω_c and the pumping rate η, which is related to the injection of photons in the cavity:

$$\left.\frac{\partial \hat{a}_\pm}{\partial t}\right|_{det} = i\omega_c \hat{a}, \quad \left.\frac{\partial \hat{a}_\pm}{\partial t}\right|_{pump} = \eta_\pm. \tag{3.5.4}$$

Adding all those rates to equation (3.5.2) we get the time derivative for the field complex amplitudes operators:

$$\frac{\mathrm{d}\hat{a}_\pm}{\mathrm{d}t} = -ig\hat{\sigma}_{12}e^{\mp ik\hat{z}} + (i\Delta_c - \kappa)\hat{a}_\pm + \eta_\pm, \tag{3.5.5}$$

where $\Delta_c = \tilde{\omega} - \omega_c$ is the light fields detuning from the cavity resonance. We consider a field with a large photon number, such that we can perform a semi-classical approximation $\langle \hat{a}_\pm \rangle = \alpha_\pm$ and $\langle \hat{z} \rangle = z$. Generalizing for N non-interacting atoms, we get a complex number derivatives

$$\dot{\alpha_\pm} = \chi\alpha_\pm - ig\sum_j^N \sigma_{12}^j e^{\mp ikz_j} + \eta_\pm, \tag{3.5.6}$$

where $\chi = (i\Delta_c - \kappa)$, while z_j and σ_{12}^j refer to the position and coherence of atom j.

Through these equations, the dynamics of the light field is related to the atomic levels coherences dynamics, which in turn depends on the light fields.

3.6 Optical forces

Let us now define the optical forces acting on each atom due to its interaction with the surrounding electric field:

$$\mathbf{F}_j = \left\langle \frac{\mathrm{d}\hat{\mathbf{p}}_j}{\mathrm{d}t} \right\rangle, \tag{3.6.1}$$

$$\frac{\mathrm{d}\hat{\mathbf{p}}}{\mathrm{d}t} = -\frac{i}{\hbar}[\hat{\mathbf{p}}, \mathcal{H}], \tag{3.6.2}$$

where we have considered only the direction of propagation $\hat{\mathbf{z}}$. From the commutators relations between $\hat{p_z}$ and $\hat{z}$ it is easy to show that

$$F_z = \frac{i}{2}\hbar k(\sigma_{12}\Theta - \sigma_{21}\Theta^*), \tag{3.6.3}$$

$$= -\hbar k \,\mathrm{Im}\{\sigma_{12}\Theta\}, \tag{3.6.4}$$

where we have defined

$$\Theta = 2g_{21}(\alpha_+ e^{ikz} - \alpha_- e^{-ikz}). \tag{3.6.5}$$

For a static atom, $\dot{z} = 0$, we can substitute the stationary solution (3.4.1) for σ_{12} to equation (3.6.4), to obtain

$$F_z = \frac{\hbar k\mathcal{D}}{|\Lambda_{21}|^2}\left(\Delta_{21}\,\mathrm{Im}\{\Omega_{21}^*\Theta\} + \frac{\Gamma_{21}}{2}\,\mathrm{Re}\{\Omega_{21}^*\Theta\}\right), \tag{3.6.6}$$

where

$$\Omega_{21}^{*}\Theta = \frac{4d_{12}^{2}\mathcal{E}^{2}}{\hbar^{2}}\Big(|\alpha_{+}|^{2} - |\alpha_{-}|^{2} + \alpha_{+}\alpha_{-}^{*}e^{2ikz} - \alpha_{+}^{*}\alpha_{-}e^{-2ikz}\Big), \tag{3.6.7}$$

$$= g_{21}^{2}\Big(|\alpha_{+}|^{2} - |\alpha_{-}|^{2} + 2i\,\mathrm{Im}\Big\{\alpha_{+}\alpha_{-}^{*}e^{2ikz}\Big\}\Big). \tag{3.6.8}$$

We can identify in equation (3.6.8) the dipolar and radiation pressure forces, considering their different behavior as functions of the detuning and decay rate. Using the definition of the stationary population difference (3.4.4), we get

$$F_{\mathrm{rad}} = g_{21}^{2}\hbar k\frac{\Gamma_{21}}{2}\frac{|\alpha_{+}|^{2} - |\alpha_{-}|^{2}}{|\Omega_{21}|^{2} + 2|\Lambda_{21}|^{2}}, \tag{3.6.9}$$

$$F_{\mathrm{dip}} = g_{21}^{2}\hbar k\Delta_{21}\frac{\alpha_{+}\alpha_{-}^{*}e^{2ikz} - \alpha_{+}^{*}\alpha_{-}e^{-2ikz}}{|\Omega_{21}|^{2} + 2|\Lambda_{21}|^{2}}, \tag{3.6.10}$$

with the total force being given by $F_z = F_{\mathrm{rad}} + F_{\mathrm{dip}}$.

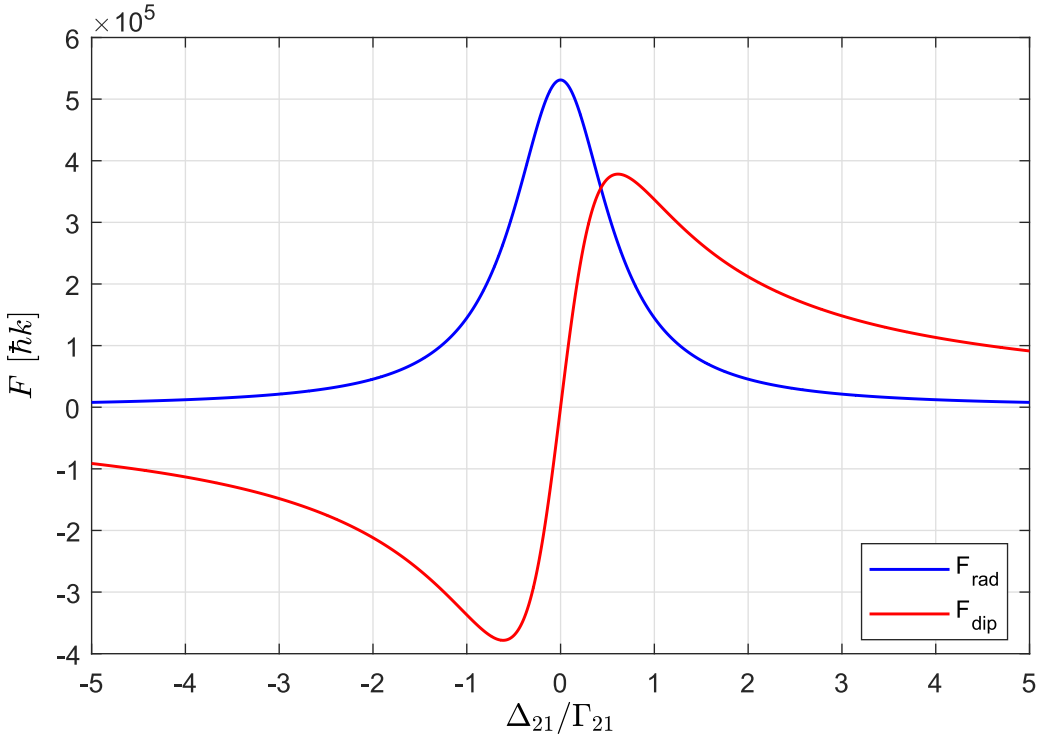

Figure 9 – Typical behaviour for the dipolar and radiative pressure forces in the two-level atom system as function of the detuning Δ_{12} for a decay rate $|\Omega_{21}| = \Gamma_{21}/2 = 10^{6}Hz$, atomic position $kz = \pi/4$ and $|\alpha_{+}| = 2|\alpha_{-}| = 100$.
Source: By the author.

In Fig. 9 we can see that the dipolar force decays slower than the radiative pressure force at high values of Δ_{21}/Γ_{21}. While the radiative pressure does not depend on the detuning sign, the dipolar force varies from repulsive to attractive as Δ_{21} changes sign

and depending on the atom position. This dependence actually leads to the grating of the atomic density. Thus the CARL phenomenon can only occur when a copropaganting field is formed in the cavity, since the dipolar force relies on a spatial modulation of the electric field.

4 THREE-LEVEL ATOM

The case we now consider is that of a three-level atom interacting with the light fields. This situation is significantly more complex than the previous one. There are three different configurations for the three atomic levels, which are denominated Lambda (Λ), V and Cascade (or Ladder Ξ):

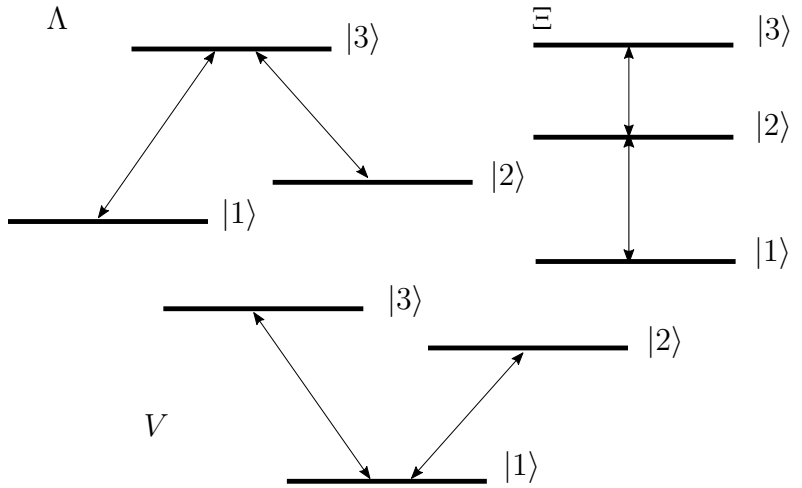

Figure 10 – Typical level configurations of a three-level atom, where each arrow represents a permitted level transition.
Source: By the author.

4.1 Bloch equations for three-level system

In this chapter, we consider a system composed of a 3LA in a cascade configuration, coupled to two light fields denominated $\mathbf{E}_{21}$ and $\mathbf{E}_{32}$, which drives the transitions of levels $|1\rangle - |2\rangle$ and $|2\rangle - |3\rangle$, respectively:

$$\vec{\mathbf{E}}_{21} = \mathrm{Re}\Big\{\mathcal{E}_{21}\Big[a_+ e^{ikz} + a_- e^{-ikz}\Big]e^{-i\tilde{\omega}t}\Big\}\hat{\mathrm{e}}, \tag{4.1.1a}$$

$$\vec{\mathbf{E}}_{32} = \mathrm{Re}\Big\{\mathcal{E}_{32} a_3 e^{-i(k_3 z + \tilde{\omega}_3 t)}\Big\}\hat{\mathrm{e}}, \tag{4.1.1b}$$

where $\mathcal{E}_{21} = i(\hbar\tilde{\omega}/2\epsilon_0 V)^{1/2}$, $\mathcal{E}_{32} = i(\hbar\tilde{\omega}_3/2\epsilon_0 V)^{1/2}$. $a_\pm$ and a_3 are the annihilation operators, k and k_3 are the wave-vectors, $\tilde{\omega}$ and $\tilde{\omega}_3$ are the mode frequencies of fields $\vec{\mathbf{E}}_{21}$ and $\vec{\mathbf{E}}_{32}$ respectively.

The total Hamiltonian in the RWA for this system becomes

$$\mathcal{H} = -\frac{\hbar^2}{2m_o}\boldsymbol{\nabla}^2 - \hbar\Delta_{21}\hat{\sigma}_{21}\hat{\sigma}_{12} - \hbar\Delta_{32}\hat{\sigma}_{32}\hat{\sigma}_{32} + \sum_{k=\pm,3}\hbar\tilde{\omega}\hat{a}_k^\dagger\hat{a}_k + \hbar g_{21}\hat{a}_\pm^\dagger e^{\pm ikz}\hat{\sigma}_{12} + \hbar g_{32}\hat{a}_3^\dagger e^{ikz}\hat{\sigma}_{32} + h.c., \tag{4.1.2}$$

where $g_{21} = d_{12}\mathcal{E}_{21}/2\hbar$ and $g_{32} = d_{23}\mathcal{E}_{32}/2\hbar$.

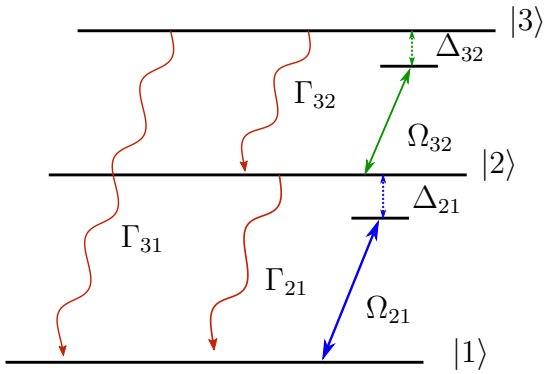

Figure 11 – Schematic representation of the atomic level system with the transitions (blue and green arrows) excited by the light fields (Ω_{21} and Ω_{32}) and the spontaneous decay transitions (red arrows) with respective decay rates (Γ).
Source: By the author.

The dipole moment (2.2.4) for the three-level atom reads:

$$\vec{\mathbf{d}} = -e(\vec{\mathbf{p}}_{12}\rho_{21} + \vec{\mathbf{p}}_{13}\rho_{31} + \vec{\mathbf{p}}_{21}\rho_{12} + \vec{\mathbf{p}}_{23}\rho_{32} + \vec{\mathbf{p}}_{31}\rho_{13} + \vec{\mathbf{p}}_{32}\rho_{23}), \tag{4.1.3}$$

$$= [d_{12}(\rho_{21} + \rho_{12}) + d_{13}(\rho_{31} + \rho_{13}) + d_{23}(\rho_{32} + \rho_{23})]\hat{\mathbf{e}}, \tag{4.1.4}$$

where we consider the electric dipole moments $\vec{\mathbf{d}}_{ij} = -e\vec{\mathbf{p}}_{\mathbf{ij}}$ in the same direction $\hat{\mathbf{e}}$ of the fields. In the cascade system we also have to consider that the transition between levels $|1\rangle$ and $|3\rangle$ is prohibited, so we can neglect d_{13} in our calculations. Thus the dipole moment simplifies into

$$\mathbf{d} = d_{12}(\rho_{21} + \rho_{12})\hat{\mathbf{e}} + d_{23}(\rho_{32} + \rho_{23})\hat{\mathbf{e}}. \tag{4.1.5}$$

Inserting the above equation in (2.4.6) and applying the ansatz of the rotating frame (3.2.1), we obtain the following equations for the diagonal density matrix elements:

$$\frac{\mathrm{d}\rho_{11}}{\mathrm{d}t} = \Gamma_{21}\rho_{22} + \frac{i}{2}(\Omega_{21}^*\sigma_{21} - \Omega_{21}\sigma_{12}), \tag{4.1.6a}$$

$$\frac{\mathrm{d}\rho_{22}}{\mathrm{d}t} = -\Gamma_{21}\rho_{22} + \Gamma_{32}\rho_{33} - \frac{i}{2}(\Omega_{21}^*\sigma_{21} - \Omega_{21}\sigma_{12}) + \frac{i}{2}(\Omega_{32}\sigma_{32} - \Omega_{32}^*\sigma_{23}), \tag{4.1.6b}$$

$$\frac{\mathrm{d}\rho_{33}}{\mathrm{d}t} = -\Gamma_{32}\rho_{33} - \frac{i}{2}(\Omega_{32}\sigma_{32} - \Omega_{32}^*\sigma_{23}). \tag{4.1.6c}$$

Then, using (3.2.1) we can derive the other density matrix elements

$$\frac{\mathrm{d}\sigma_{12}}{\mathrm{d}t} = -\tfrac{i}{2}\Omega_{21}^*(\rho_{11} - \rho_{22}) - \Lambda_{21}\sigma_{12} - \tfrac{i}{2}\Omega_{32}\sigma_{13}, \tag{4.1.6d}$$

$$\frac{\mathrm{d}\sigma_{13}}{\mathrm{d}t} = -\tfrac{i}{2}\Omega_{32}^*\sigma_{12} - \Lambda_{31}\sigma_{13} + \tfrac{i}{2}\Omega_{21}^*\sigma_{23}, \tag{4.1.6e}$$

$$\frac{\mathrm{d}\sigma_{23}}{\mathrm{d}t} = -\tfrac{i}{2}\Omega_{32}^*(\rho_{22} - \rho_{33}) + \tfrac{i}{2}\Omega_{21}\sigma_{13} - \Lambda_{32}\sigma_{23}, \tag{4.1.6f}$$

where we define the generalized Rabi frequencies for the fields as:

$$\Omega_{21} = \frac{d_{12}E_{21}}{\hbar}, \tag{4.1.7}$$

$$\Omega_{32} = \frac{d_{23}E_{32}}{\hbar}. \tag{4.1.8}$$

For the cascade configuration, we define $\Lambda_{21} = \frac{1}{2}\Gamma_{21} + i\Delta_{21}$, $\Lambda_{32} = \frac{1}{2}(\Gamma_{21} + \Gamma_{31} + \Gamma_{32}) + i\Delta_{32}$ and $\Lambda_{31} = \frac{1}{2}(\Gamma_{31} + \Gamma_{32}) + i(\Delta_{21} + \Delta_{32})$, with $\Delta_{ij} = \tilde{\omega} - \omega_{ij}$ the frequency detuning between the $|\psi_i\rangle$-$|\psi_j\rangle$ transitions and the respective exciting field.

We can represent the above equations system in a matrix form

$$\dot{\vec{\rho}} = \mathcal{L} \cdot \vec{\rho}, \tag{4.1.9}$$

where we introduce the following vector with the density matrix elements

$$\vec{\rho} = \begin{pmatrix} \rho_{11} & \rho_{22} & \rho_{33} & \sigma_{12} & \sigma_{21} & \sigma_{13} & \sigma_{31} & \sigma_{23} & \sigma_{32} \end{pmatrix}^T, \tag{4.1.10}$$

$$\mathcal{L} = \begin{pmatrix} 0 & \Gamma_{21} & \Gamma_{31} & -\frac{i}{2}\Omega_{21} & \frac{i}{2}\Omega_{21}^* & 0 & 0 & 0 & 0 \\ 0 & -\Gamma_{21} & \Gamma_{32} & \frac{i}{2}\Omega_{21} & -\frac{i}{2}\Omega_{21}^* & 0 & 0 & -\frac{i}{2}\Omega_{32} & \frac{i}{2}\Omega_{32}^* \\ 0 & 0 & -\Gamma_{32} - \Gamma_{31} & 0 & 0 & 0 & 0 & \frac{i}{2}\Omega_{32} & -\frac{i}{2}\Omega_{32}^* \\ -\frac{i}{2}\Omega_{21}^* & \frac{i}{2}\Omega_{21}^* & 0 & -\Lambda_{21} & 0 & -\frac{i}{2}\Omega_{32} & 0 & 0 & 0 \\ \frac{i}{2}\Omega_{21} & -\frac{i}{2}\Omega_{21} & 0 & 0 & -\Lambda_{21}^* & 0 & \frac{i}{2}\Omega_{32}^* & 0 & 0 \\ 0 & 0 & 0 & -\frac{i}{2}\Omega_{32}^* & 0 & -\Lambda_{31} & 0 & \frac{i}{2}\Omega_{21}^* & 0 \\ 0 & 0 & 0 & 0 & \frac{i}{2}\Omega_{32} & 0 & -\Lambda_{31}^* & 0 & -\frac{i}{2}\Omega_{21} \\ 0 & -\frac{i}{2}\Omega_{32}^* & \frac{i}{2}\Omega_{32}^* & 0 & 0 & \frac{i}{2}\Omega_{21} & 0 & -\Lambda_{32} & 0 \\ 0 & \frac{i}{2}\Omega_{32} & -\frac{i}{2}\Omega_{32} & 0 & 0 & 0 & -\frac{i}{2}\Omega_{21}^* & 0 & -\Lambda_{32}^* \end{pmatrix}. \tag{4.1.11}$$

4.2 Stationary case

Focusing on the off-diagonal terms of the density matrix (i.e. the coherences), we can write the following linear system

$$\begin{pmatrix} \dot{\sigma_{12}} \\ \dot{\sigma_{13}} \\ \dot{\sigma_{23}} \end{pmatrix} = \begin{pmatrix} -\Lambda_{21} & -\frac{i}{2}\Omega_{32} & 0 \\ -\frac{i}{2}\Omega_{32}^* & -\Lambda_{31} & \frac{i}{2}\Omega_{21}^* \\ 0 & \frac{i}{2}\Omega_{21} & -\Lambda_{32} \end{pmatrix} \begin{pmatrix} \sigma_{12} \\ \sigma_{13} \\ \sigma_{23} \end{pmatrix} + \begin{pmatrix} -\frac{i}{2}\Omega_{21}^*(\rho_{11} - \rho_{22}) \\ 0 \\ -\frac{i}{2}\Omega_{32}^*(\rho_{22} - \rho_{33}) \end{pmatrix}. \tag{4.2.1}$$

This allows us to obtain the stationary solution for the coherences as functions of the populations, by setting the left-hand term to zero, and using the condition $\rho_{11} + \rho_{22} + \rho_{33} = 1$.

We then obtain the following expressions

$$\sigma_{12} = \frac{i\Omega_{21}}{2} \frac{\left[\rho_{22}(2\Xi_3 - |\Omega_{32}|^2) + \rho_{33}(\Xi_3 + |\Omega_{32}|^2) - \Xi_3\right]}{\Lambda_{32}|\Omega_{32}|^2 + \Lambda_{21}|\Omega_{21}|^2 + 4\Lambda_{21}\Lambda_{31}\Lambda_{32}}, \tag{4.2.2a}$$

$$\sigma_{13} = \Omega_{21}\Omega_{32} \frac{\left[\rho_{22}(2\Lambda_{32} + \Lambda_{21}) + \rho_{33}(\Lambda_{32} - \Lambda_{21}) - \Lambda_{32}\right]}{\Lambda_{32}|\Omega_{32}|^2 + \Lambda_{21}|\Omega_{21}|^2 + 4\Lambda_{21}\Lambda_{31}\Lambda_{32}}, \tag{4.2.2b}$$

$$\sigma_{23} = \frac{i\Omega_{32}}{2} \frac{\left[\rho_{22}(2|\Omega_{21}|^2 - \Xi_2) + \rho_{33}(\Xi_2 + |\Omega_{21}|^2) - |\Omega_{21}|^2\right]}{\Lambda_{32}|\Omega_{32}|^2 + \Lambda_{21}|\Omega_{21}|^2 + 4\Lambda_{21}\Lambda_{31}\Lambda_{32}}, \tag{4.2.2c}$$

where we have defined

$$\Xi_2 = |\Omega_{32}|^2 + 4\Lambda_{21}\Lambda_{31},$$
$$\Xi_3 = |\Omega_{21}|^2 + 4\Lambda_{32}\Lambda_{31}.$$

4.3 Optical Fields

Analogous to section 3.5 we derive the equations for the cavity light fields dynamics from the Hamiltonian in the RWA. Focusing on the time evolution of the cavity modes $\alpha_\pm$, their derivatives, in presence of losses (cavity decay rate κ) and pump ($\eta_\pm$), are given by

$$\dot{\alpha}_\pm = ig_{21}\left\langle \sigma_{12}e^{-ikz_j}\right\rangle + (i\Delta_c - \kappa)\alpha_\pm + \eta_+, \tag{4.3.1}$$

where we obtain the same expression as in equation (3.5) since each exciting field does not couple with the coherence of other transitions.

Throughout this project, we consider the light field mode α_3 constant and neglect any variation during the system dynamics.

4.4 Optical Forces

As in section 3.6, we can derive the optical forces on each atom from the Hamiltonian (4.1.2). With the definition of Θ in (3.6.5) we can write the optical force for the 3LA as

$$F_{z_j} = \tfrac{i}{2}\hbar k(\sigma_{12}\Theta - \sigma_{21}\Theta^*) + \tfrac{i}{2}\hbar k_3(\sigma_{23}\Omega_{32} - \sigma_{32}\Omega_{32}^*), \tag{4.4.1}$$
$$F_{z_j} = -\hbar k\,\mathrm{Im}\{\sigma_{12}\Theta\} - \hbar k_3\,\mathrm{Im}\{\sigma_{23}\Omega_{32}\}. \tag{4.4.2}$$

In the case of a 3LA the steady-state expressions for σ_{21} and σ_{32} are very complex, so we do not write them explicitly.

5 ELECTROMAGNETIC INDUCED TRANSPARENCY - EIT

In this chapter, we focus on the optical properties of atomic clouds and discuss how they can be tuned taking advantage of the third level of the atoms.[21–23]

By inducing atomic coherences with a laser, we can cause quantum interference between the different pathways in the energy level structure, which affects the material optical response. This way, it is actually even possible to reduce or even eliminate the absorption of a transition. This phenomenon, called electromagnetic induced transparency (EIT), was demonstrated for the first time in a strontium gas[24] where, by applying a strong coupling field between a metastable state and the upper state of a permitted transition, it was possible to obtain induced transparency in the material.

The main objective of studying this effect in our system is the intrinsic relation between the optical forces exerted by the light fields on the atoms and its transition coherences as in equations (4.4.2). Our objective is to understand if the manipulation of the atomic coherences could lead to a reduction in the radiative pressure force exerted on the atoms.

5.1 Static description of EIT

To observe the EIT phenomenon, one needs at least two different transitions, as in a three-level system analysed in chapter 4. By making the distinction between the similar phenomenon of AT (Autler-Townes splitting),[25] we can only select between a Lambda and Cascade configuration to study the EIT. In this work we choose the Cascade.

Let us consider the trapped atomic cloud inside the ring cavity, interacting with

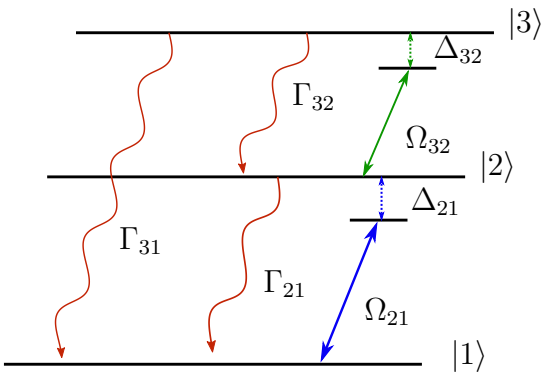

Figure 12 – Schematic representation of the Cascade three-level level system with the transitions (blue and green arrows) excited by the light fields Ω_{21} and Ω_{32}, and the spontaneous decay transitions (red arrows) with respective decay rates $\Gamma_{21}, \Gamma_{32}, \Gamma_{31}$, where the last one can be neglected in our system.
Source: By the author.

two light field ($\mathbf{E}_{21}$ and $\mathbf{E}_{32}$), as described in equation (4.1.1). The interaction Hamiltonian for this system can be written in the RWA as

$$\mathcal{H}_{int} = \frac{\hbar}{2}\begin{pmatrix} 0 & \Omega_{21}^* & 0 \\ \Omega_{21} & 2\Delta_{21} & \Omega_{32}^* \\ 0 & \Omega_{32} & 2(\Delta_{21}+\Delta_{23}) \end{pmatrix}, \tag{5.1.1}$$

whose parameters were defined in chapter 4.

Although diagonalizing the Hamiltonian in the general case leads to complex expressions, in the resonant case $\Delta_{21}+\Delta_{23}=0$ it is straightforward to obtain the following eigenvalues

$$\hbar\omega^0 = 0, \tag{5.1.2}$$

$$\hbar\omega^+ = \Delta_{21} + \sqrt{\Delta_{21}^2 + |\Omega_{21}|^2 + |\Omega_{32}|^2}, \tag{5.1.3}$$

$$\hbar\omega^- = \Delta_{21} - \sqrt{\Delta_{21}^2 + |\Omega_{21}|^2 + |\Omega_{32}|^2}, \tag{5.1.4}$$

which are associated to the following eigenstates:

$$|0\rangle = \frac{\Omega_{23}^*}{\Omega}|1\rangle - \frac{\Omega_{12}}{\Omega}|3\rangle, \tag{5.1.5}$$

$$|+\rangle = \frac{\Omega_{12}^*}{\Omega}\sin\theta\,|1\rangle + \cos\theta\,|2\rangle + \frac{\Omega_{23}}{\Omega}\sin\theta\,|3\rangle, \tag{5.1.6}$$

$$|-\rangle = \frac{\Omega_{12}^*}{\Omega}\cos\theta\,|1\rangle - \sin\theta\,|2\rangle + \frac{\Omega_{23}}{\Omega}\cos\theta\,|1\rangle, \tag{5.1.7}$$

where we have introduced θ such as

$$\sin 2\theta = \frac{\sqrt{|\Omega_{21}|^2 + |\Omega_{32}|^2}}{\sqrt{\Delta_{21}^2 + |\Omega_{21}|^2 + |\Omega_{32}|^2}}, \tag{5.1.8}$$

$$\cos 2\theta = \frac{\Delta_{12}}{\sqrt{\Delta_{21}^2 + |\Omega_{21}|^2 + |\Omega_{32}|^2}}. \tag{5.1.9}$$

State $|0\rangle$ is called a *dark state* since it does not interact with the light fields, i.e., it is not coupled to the atomic eigenstate $|2\rangle$. This provides a basic understanding of the EIT: the driven field sends the atom to a dark state, where an interaction with the probe light is no longer possible. As a result, it behaves as a transparent medium.

However, this description is oversimplified since it disregards the influence of spontaneous emission, whose treatment requires a density matrix formalism as derived in chapter 4.

5.2 EIT in presence of spontaneous emission

The steady state solutions for the 3LA coherences (density matrix off-diagonal elements) were obtained in section 4.2. In this chapter we focus only on the coherence

σ_{12} of the $|1\rangle \rightarrow |2\rangle$ transition. Although its expression is cumbersome, we can simplify equation (4.2.2a) by considering that the transition $|2\rangle$-$|3\rangle$ is driven at resonance ($\Delta_{32} = 0$), and by neglecting the excited populations ($\rho_{22} \approx \rho_{33} \approx 0$):

$$\sigma_{12} = -i\Omega_{21}\frac{\Xi_3}{(\Gamma_{23}+\Gamma_{21})|\Omega_{32}|^2 + (\Gamma_{21}+2i\Delta_{21})\Xi_3},$$
$$\sigma_{12} = \frac{-i\Omega_{21}}{\frac{|\Omega_{32}|^2}{\frac{|\Omega_{21}|^2}{(\Gamma_{23}+\Gamma_{21})}+2\Lambda_{21}}} + 2\Lambda_{21}, \tag{5.2.1}$$

where $\Xi_3 = |\Omega_{21}|^2 + (\Gamma_{23}+\Gamma_{21})(\Gamma_{21}+2i\Delta_{21})$. Finally, since we considered that the transition between levels $|1\rangle$ and $|3\rangle$ is prohibited, this allow us to neglect its decay rate, $\Gamma_{31} = 0$. Comparing to the case where $\Omega_{32} = 0$, we can expect new resonant peaks in both real and imaginary parts of σ_{12}, as can be observed in Fig. 13: it depicts the real and imaginary part of σ_{12} as a function of the detuning for transition $|1\rangle$-$|2\rangle$, for different ratios between the Rabi frequencies, Ω_{32}/Ω_{21}.

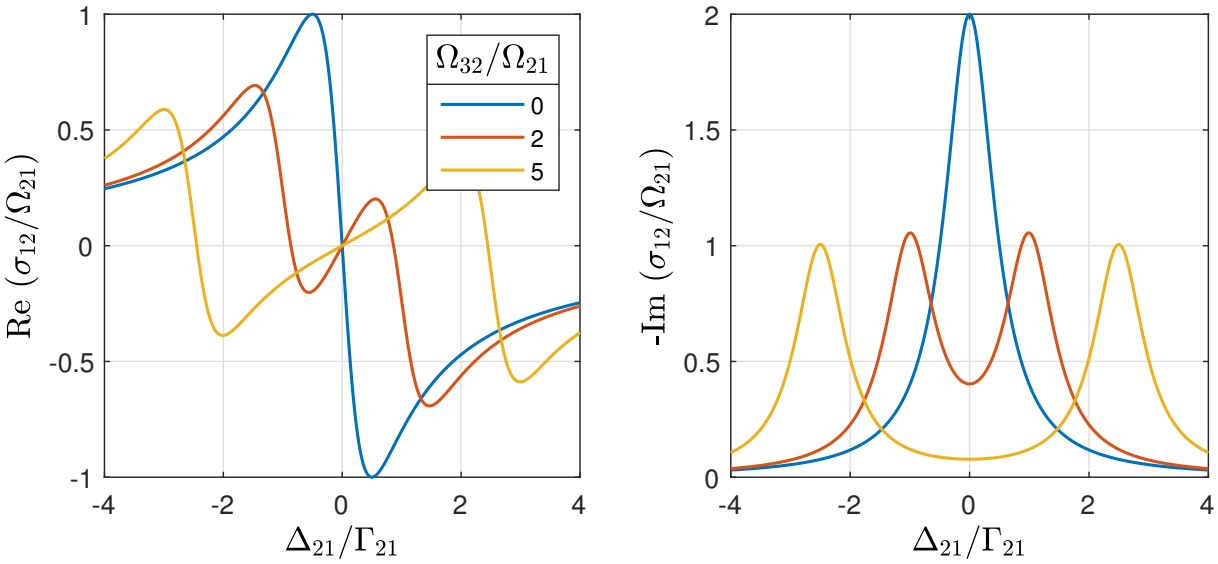

Figure 13 – Real and imaginary parts of the 3LA coherence σ_{12} as a function of the detuning of the transition $|1\rangle \rightarrow |2\rangle$ for different pumping strengths Ω_{32} of transition $|2\rangle \rightarrow |3\rangle$. Parameters for the figure are $\Gamma_{32} = 0.1\Gamma_{21}$ and $\Omega_{21} = \Gamma_{21}$. Source: By the author.

As expected, the curves for $\Omega_{32} = 0$ in Fig. 13 are the same as those of the dipolar and radiative pressure forces in 3.6, since we recover the two-level atom case. The behavior of the coherence near resonance is what instigates us to analyse the EIT phenomenon, since at high ratios of Ω_{32}/Ω_{21} the imaginary part of σ_{12} (related to the radiative pressure force), reaches lower values than the real part (related to the dipolar force). However, these new peaks only occur when the decay rate Γ_{32} is smaller than Γ_{21}, and the resonances for σ_{21} only get broader, see Fig. 14, since the third level decays rapidly after being excited from the second level, and the system behaves as a two-level atom.

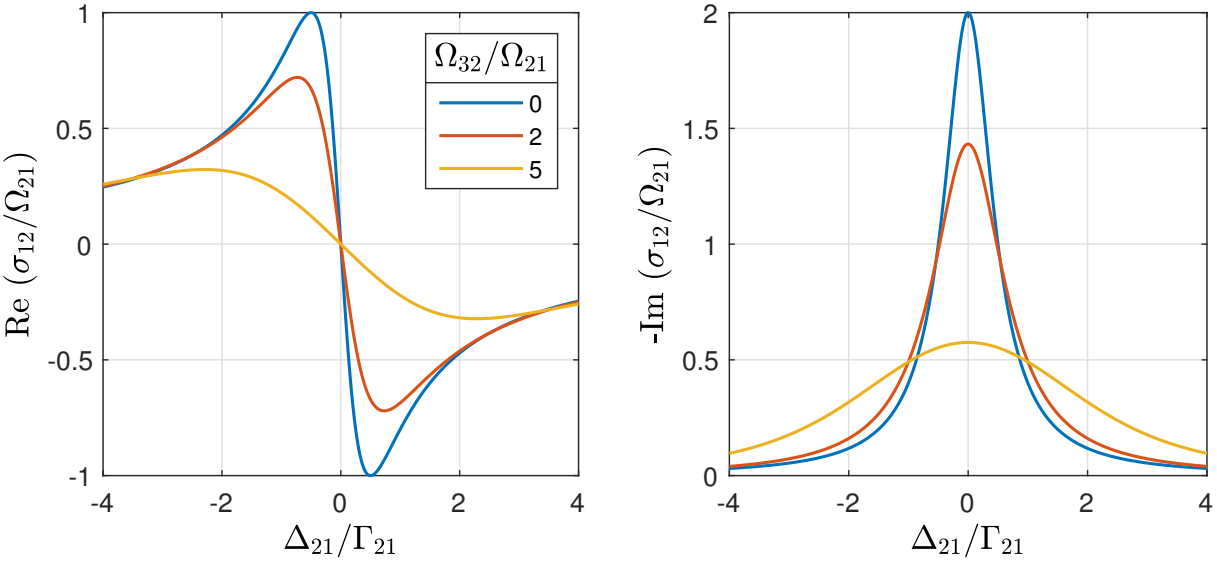

Figure 14 – Real and imaginary parts of the 3LA coherence σ_{12} as a function of the detuning of the transition $|1\rangle \rightarrow |2\rangle$ for different pumping strengths Ω_{32} of transition $|2\rangle \rightarrow |3\rangle$. Parameters for the figure are $\Gamma_{32} = 10\Gamma_{21}$ and $\Omega_{21} = \Gamma_{21}$.
Source: By the author.

Since the assumption of negligible excited populations is not valid for the near-resonance regime ($\Omega_{21}^2/(\Gamma_{21}^2 + 4\Delta_{21}^2)$ not negligible), we analyse the system using the full optical Bloch equations (4.2.2) for the steady state. In Fig. 15 we reproduce the new resonant peaks and gaps in the coherence as in Fig. 13 at higher values of Ω_{21}, throughout a larger region of Δ_{21}.

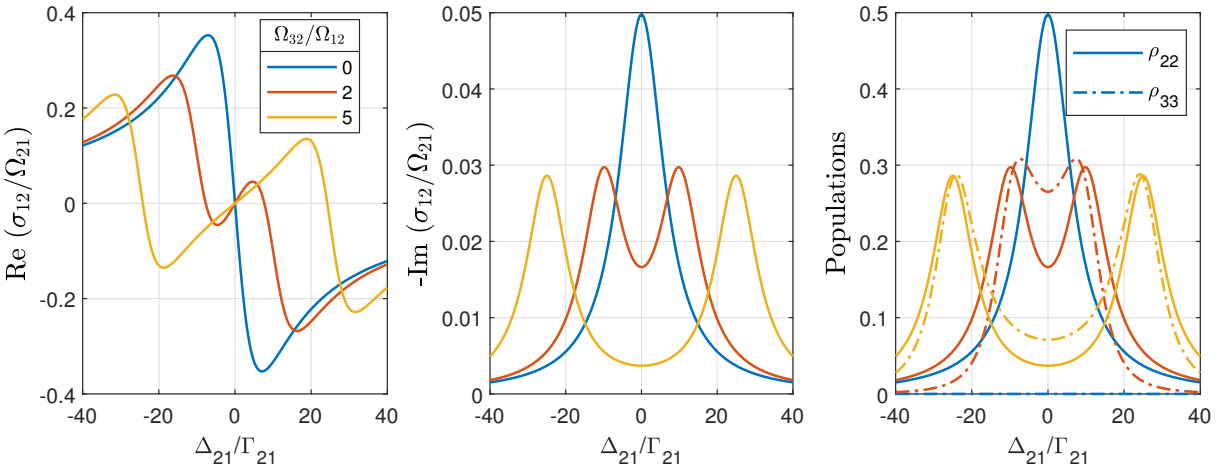

Figure 15 – Real and imaginary parts of the coherence σ_{12} as a function of the detuning for the complete steady state Bloch equations and excited levels populations. Parameters for the figure are $\Gamma_{32} = \Gamma_{21}$ and $\Omega_{21} = 10\Gamma_{21}$. In the right picture, for $\Omega_3 2/\Omega_1 2 = 0$, $\rho_3 3 = 0$ (i.e., the dash-dotted blue curve overlaps with the x-axis)
Source: By the author.

For a decay rate Γ_{32} lower than Γ_{21} the imaginary part of σ_{12} reaches values closer to zero, see figure 16. This effect is not captured by equation (5.2.1), which neglects the

excited populations.

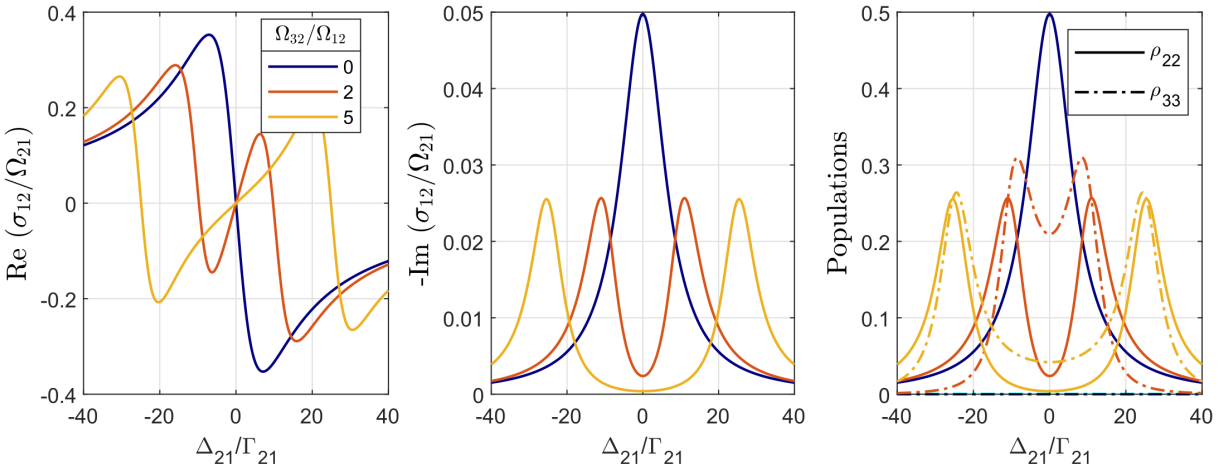

Figure 16 – Real and imaginary parts of the coherence σ_{12} as a function of the detuning for the complete steady state Bloch equations and excited levels populations. Parameters for the figure are $\Gamma_{32} = 0.1\Gamma_{21}$ and $\Omega_{21} = 10\Gamma_{21}$.
Source: By the author.

The most interesting characteristic of the depicted curves is that for a large ratio between the light field strengths, the real part of σ_{12} decays slower than the imaginary part near the resonance, as it happens in the far-from-resonance regime for any value of Ω_{32}. This means that the dipolar force influence in the atomic dynamics can be stronger than the radiative pressure force near resonance due to the EIT.

We also note that the excited populations are largely reduced near resonance, see right graphic in Fig. 16 (i.e., at large detunings, the dipolar force dominates over the radiation pressure one). Such behavior can be exploited in the context of the adiabatic elimination, where the excited levels are eliminated from the dynamics when the light field is far detuned. Our results suggest that this effect can be achieved close to resonance using the EIT scheme.

5.3 Radiative pressure force reduction

From the above results we can infer that in the EIT regime the imaginary part of σ_{12} is reduced in relation to its real part. Since from equation (3.6.4) we can associate the imaginary and real part of the coherence with the radiative pressure and dipolar force, respectively, therefore we can expect a large ratio between these forces near the resonance of transition $|1\rangle$-$|2\rangle$. However, it is only possible to obtain values of the ratio $|\mathrm{Re}\,\sigma_{12}/\,\mathrm{Im}\,\sigma_{12}|$ greater than the usual ratio (i.e., in absence of third level: $\Omega_{32} = 0$), when the decay rate Γ_{32} is lower than Γ_{21}. In Fig. 17 we can note that for $\Gamma_{32}/\Gamma_{21} = 10$, the ratio resembles a parabola, which is due to the absence of the resonant peaks in this case, as in Fig. 14.

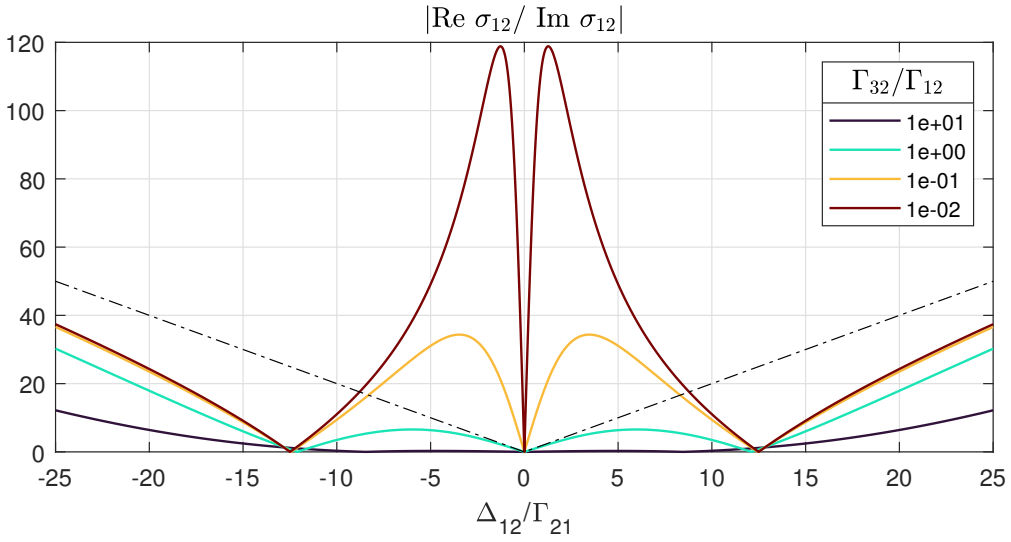

Figure 17 – Ratio between real and imaginary parts of the transition $|1\rangle$-$|2\rangle$ coherence, varying the values of the decay rate for the transition $|2\rangle$-$|3\rangle$. Here we have used $\Omega_{32} = 5\Omega_{21}$ and $\Omega_{21} = 5\Gamma_{21}$. The black dashed line is the solution for $\Omega_{23} = 0$.

Source: By the author.

Using equation (4.4.2) we can analyse the influence of EIT on the optical forces, analogously to the analysis made for the coherence in the previous section. By considering different atomic positions and different values for the counterpropagating cavity modes as in expression (3.6.8), it is possible to calculate separately the dipolar and radiative pressure forces.

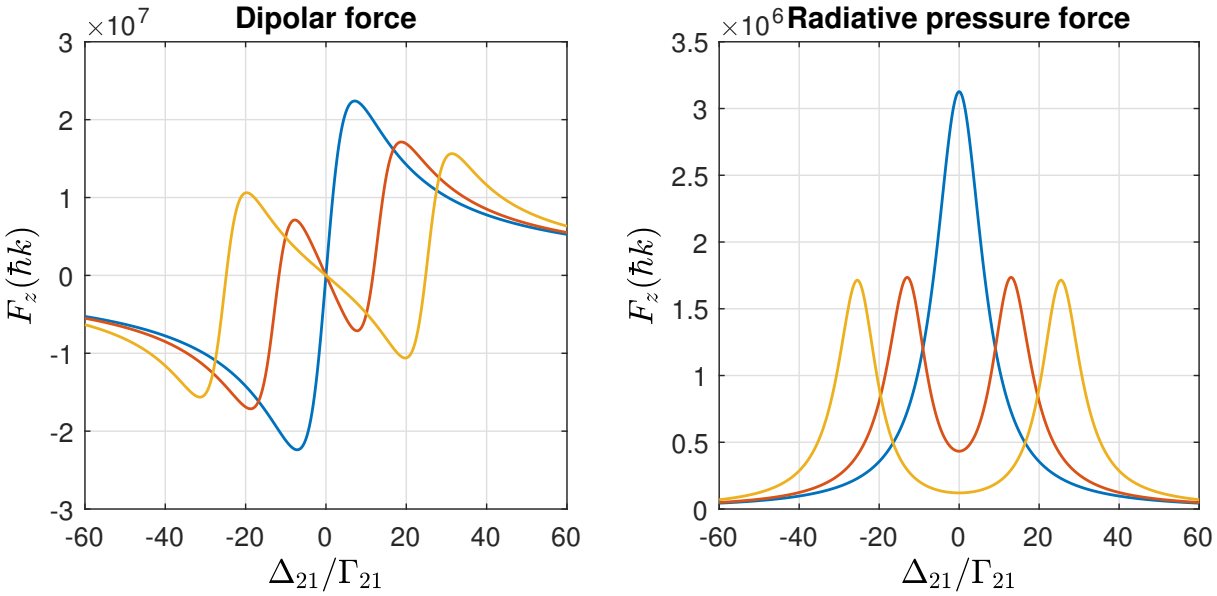

Figure 18 – New resonant peaks in the optical forces steady state solutions, as functions of the transition $|1\rangle$-$|2\rangle$ detuning for different transition $|2\rangle$-$|3\rangle$ Rabi frequencies. Parameters for the figure are $\Gamma_{32} = 0.1\Gamma_{21}$ and $\Omega_{12} = 10\Gamma_{21}$.

Source: By the author.

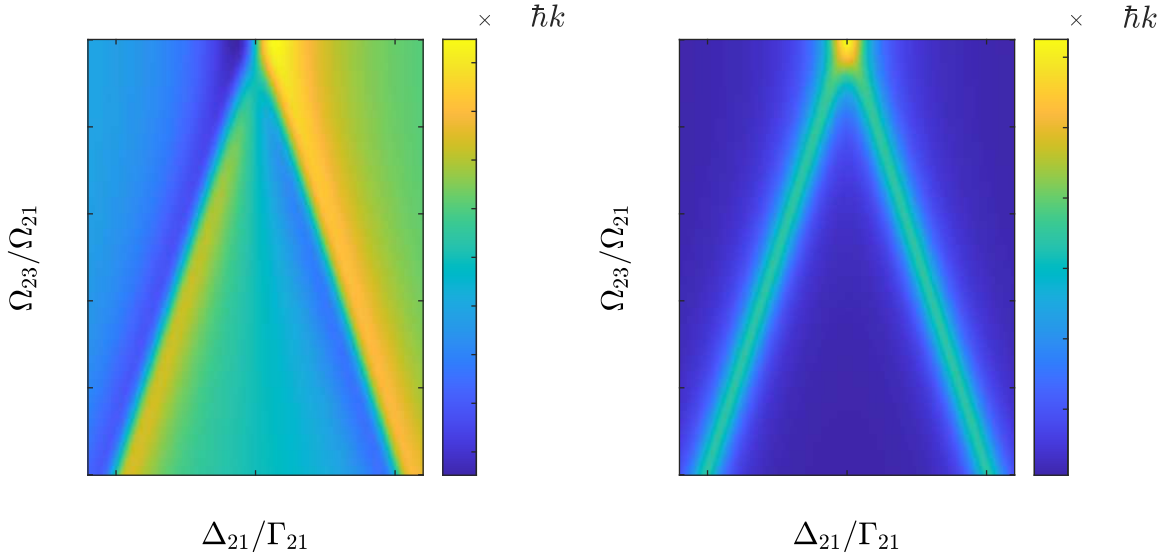

Figure 19 – Optical forces in $\hbar k$ as function of transition $|1\rangle$-$|2\rangle$ detuning and pump strength of transition $|2\rangle$-$|3\rangle$. Parameters for the figures are $\Gamma_{32} = 0.5\Gamma_{21}$ and $\Omega_{12} = 10\Gamma_{21}$.

Source: By the author.

In Fig. 18 we present the new resonant peaks for each optical force obtained by the steady state solution of σ_{12}. Near resonance, we obtain a dipole force larger than the radiative pressure for large value of Ω_{32}/Ω_{21}, along with an inversion of sign related to the detuning Δ_{21}, which means that the forces becomes repulsive in a region where it would be attractive without the EIT. Increasing the value o Ω_{32} we can see that those peaks grow apart for both forces, see Fig. 19, where we calculate each force as a function of both Δ_{21} and Ω_{32}.

We determine the regions where the radiative pressure force is reduced enough so its dissipative effect on the atoms is lower than the dynamical effect of the dipolar force, by monitoring the ratio between those force $|F_{\text{dip}}/F_{\text{rad}}|$. In Fig. 20 we can note that large values of this ratio are available near-resonance in the EIT regime, while such values would occur only at far resonance regions without the pumping of transition $|2\rangle$-$|3\rangle$ (yet far from resonance, the forces are much weaker). In Fig. 21 we show the forces ratio for a weaker light-atom coupling Ω_{21} of transition $|1\rangle$-$|2\rangle$, which requires a lower decay rate and higher pump strength of transition $|2\rangle$-$|3\rangle$ to suppress the radiative pressure force.

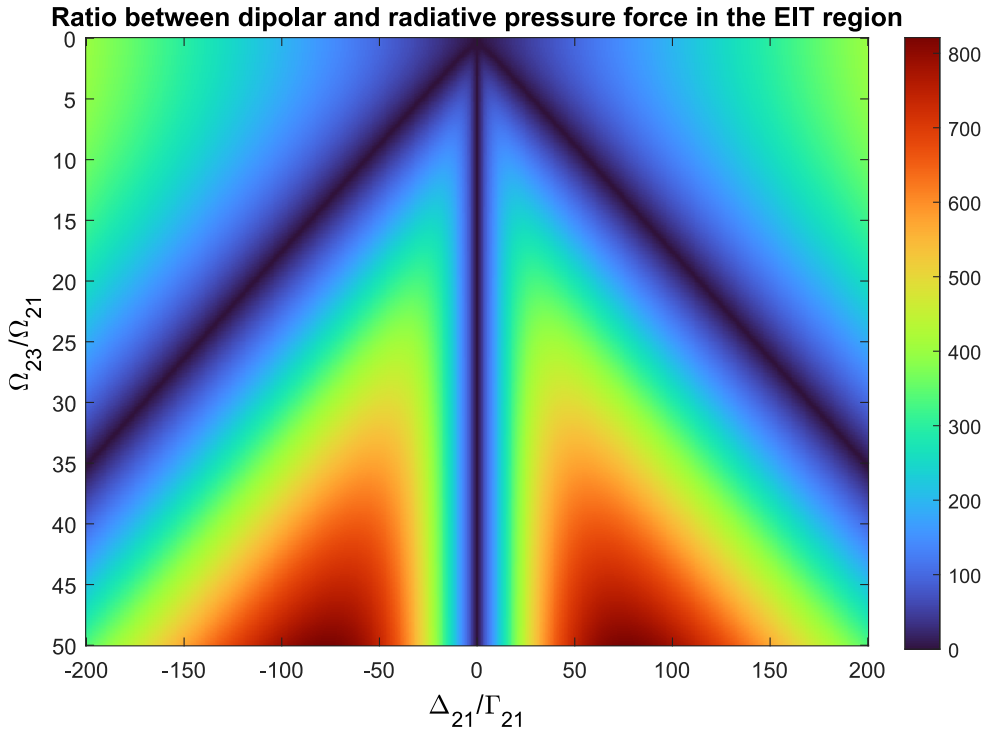

Figure 20 – Ratio between dipolar and radiative force as function of transition $|1\rangle$-$|2\rangle$ detuning and pump strength of transition $|2\rangle$-$|3\rangle$. Parameters for the figure are $\Gamma_{32} = 0.1\Gamma_{21}$ and $\Omega_{12} = 10\Gamma_{21}$.
Source: By the author.

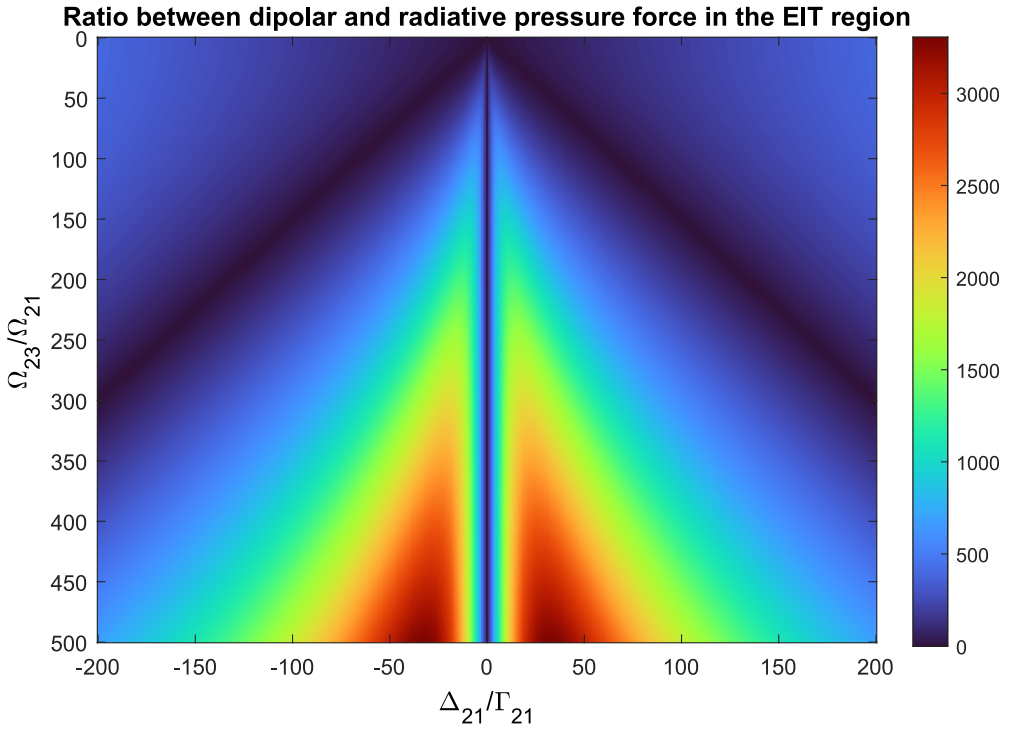

Figure 21 – Ratio between dipolar and radiative force as function of transition $|1\rangle$-$|2\rangle$ detuning and pump strength of transition $|2\rangle$-$|3\rangle$. Parameters for the figure are $\Gamma_{32} = 0.01\Gamma_{21}$ and $\Omega_{12} = 1\Gamma_{21}$.
Source: By the author.

6 MATTER-WAVES AND REPRESENTATION IN MOMENTUM SPACE

In the previous chapters we have showed that the EIT effect depends only on the internal atom dynamics, which so far has allowed us to analyse the system equations using only its internal degrees of freedom. However, it is now necessary to consider extended atoms to observe the Bloch oscillations, where the exchange of momentum between atoms and light fields occur at integers values of photon momentum.

In this chapter we introduce this formalism using the quantization of the momentum operator, considering an atomic matter wave, and derive the optical Bloch equations for the two- and three-level atom systems, including the optical lattice and external force as required to observe the Bloch oscillations.

6.1 Quantum momentum operator

The Hamiltonian of the atomic matter wave interacting with two different light fields, within the dipole approximation and RWA, consists of the following contributions

$$\mathcal{H}_{atom} = \frac{\hat{p}^2}{2m_o} - \hbar\Delta_{21}\hat{\sigma}_{21}\hat{\sigma}_{12} - \hbar\Delta_{32}\hat{\sigma}_{32}\hat{\sigma}_{23}, \tag{6.1.1a}$$

$$\mathcal{H}_{int} = \hbar g_{21}\left(\hat{a}_+^\dagger e^{-ik\hat{z}} + \hat{a}_-^\dagger e^{ik\hat{z}}\right)\hat{\sigma}_{12} + \hbar g_{32}\hat{a}_3^\dagger e^{-ik_3\hat{z}}\hat{\sigma}_{23} + h.c., \tag{6.1.1b}$$

$$\mathcal{H}_{field} = -\hbar\Delta_c\hat{a}_q^\dagger\hat{a}_q, \tag{6.1.1c}$$

where $g_{ij} = d_{ij}\mathcal{E}_{ij}/2\hbar$ is the light-atom coupling strength, also called the single-photon Rabi frequency.

If the atomic sample is much larger than the radiation wavelength, and its density is uniform, the atomic wave function $\Psi(\hat{\mathbf{r}}, t)$ can be expanded into plane waves in the cavity axis $\hat{\mathbf{z}}$, with periodicity of kz

$$\Psi(\hat{\mathbf{r}}, t) = \sum_n \sum_j c_{j,n}\psi_j(\hat{\mathbf{r}})e^{inkz}, \tag{6.1.2}$$

where ψ_j are the unperturbed Hamiltonian eigenstates, and $|c_{j,n}|^2$ the probability of finding the atoms in the n-th momentum state and j-th atomic state ($j = 1, 2, 3$ for a three-level system).

The momentum quantization along the z-axis is realized by the definition of the momentum operator $\hat{\mathbf{p}}$, whose expectation value only assumes integer multiples of $\hbar k$:

$$\hat{p}_z = \sum_n n\hbar k \left|n\right\rangle\!\left\langle n\right|, \tag{6.1.3}$$

where $\langle \mathbf{r}|n\rangle = e^{inkz}$ is the momentum eigenstate. From the momentum and position commutator $[\hat{z},\hat{p}] = i\hbar$, we can derive the momentum kick-operator as

$$e^{ik\hat{z}} = \sum_n |n+1\rangle\langle n|\,, \quad e^{-ik\hat{z}} = \sum_n |n-1\rangle\langle n|\,. \tag{6.1.4}$$

Using the Dirac notation we can rewrite the atomic wave function as

$$|\Psi(t)\rangle = \sum_{n=-\infty}^{\infty}\sum_{j}^{3} c_{j,n}\,|j,n\rangle\,, \tag{6.1.5}$$

where $|j,n\rangle = |j\rangle \otimes |n\rangle$, and $\langle \mathbf{r}|j\rangle = \psi_j(\hat{\mathbf{r}})$ is the atomic Hamiltonian eigenstate. The normalization condition of $|\Psi\rangle$ gives us the atoms number N in the matter wave as

$$\langle \Psi(t)|\Psi(t)\rangle = N. \tag{6.1.6}$$

We can add the optical lattice contribution to the system through the term $\hbar W_o \sin(2kz)/2$, which describes a stationary wave with periodicity of $2kz$. This stationary wave can be generated by two laser beams crossing the cavity at a determined angle, see Fig. 4. Expanding the sine,

$$\mathcal{H}_{latt} = \frac{\hbar W_o}{2}\sin(2k\hat{z}) = -i\hbar\frac{W_o}{4}\Big(e^{2ik\hat{z}} - e^{-2ik\hat{z}}\Big), \tag{6.1.7}$$

we can see that the optical lattice contribution to the system are the momentum kick operators, which change the atoms momentum in integers values of $\pm 2\hbar k$.

The gravity force acting on the atoms can be included in the atomic Hamiltonian (6.1.1a) by potential $V(\hat{\mathbf{r}}) = m_o g\hat{\mathbf{r}}$, where $\hat{\mathbf{r}}$ is the atom position operator and g is the gravity acceleration. To simplify the equations we consider the movement of the atom only in the $\hat{\mathbf{z}}$ direction and describe the dynamics of the system in a accelerated frame moving with momentum $m_o g t$ in the positive direction of the z-axis. The atom wave-function in this frame is transformed as

$$\Psi = \tilde{\Psi} e^{im_o g z t/\hbar}, \tag{6.1.8}$$

which is given by the free-fall solution of Ψ in this potential. The Schrödinger equation for the atomic wave-function then reads

$$i\hbar\frac{\mathrm{d}\Psi}{\mathrm{d}t} = \mathcal{H}_{atom}\Psi, \tag{6.1.9}$$

$$i\hbar\frac{\mathrm{d}\tilde{\Psi}}{\mathrm{d}t}e^{im_o g z t/\hbar} - m_o g z\Psi = -\frac{\hbar^2 k^2}{2m_o}\frac{\partial^2}{\partial z^2}\Big(\tilde{\Psi}e^{im_o g z t/\hbar}\Big) - m_o g z\Psi, \tag{6.1.10}$$

$$i\hbar\frac{\mathrm{d}\tilde{\Psi}}{\mathrm{d}t} = -\frac{\hbar^2 k^2}{2m_o}\left(\frac{\partial}{\partial z} + \frac{im_o g t}{\hbar}\right)^2\tilde{\Psi}. \tag{6.1.11}$$

Finally the atomic Hamiltonian in the accelerated frame can be written as

$$\tilde{\mathcal{H}}_{atom} = -\frac{\hbar^2 k^2}{2m_o}\left(\frac{\hat{p}}{\hbar k} + \frac{im_o g t}{\hbar}\right)^2. \tag{6.1.12}$$

6.2 Schrödinger equation for the two-level atoms

We can start analysing the system for the two-level atom case in the Schrödinger equation picture by neglecting the spontaneous emission. The derivatives of the complex amplitudes in eq. (6.1.2) turn into the following set of coupled differential equations

$$\dot{c}_{1,n} = -i\omega_r(n+2\nu_b t)^2 c_{1,n} + ig_{21}\Big(\alpha_+^* c_{2,n+1} + \alpha_-^* c_{2,n-1}\Big) + \tfrac{W_o}{4}(c_{1,n+2} - c_{1,n-2}), \quad (6.2.1a)$$

$$\dot{c}_{2,n} = -i\omega_r(n+2\nu_b t)^2 c_{2,n} - i\Delta_{21} c_{2,n} + ig_{21}(\alpha_+ c_{1,n-1} + \alpha_- c_{1,n+1}) + \tfrac{W_o}{4}(c_{2,n+2} - c_{2,n-2}), \quad (6.2.1b)$$

where $\omega_r = \hbar k^2/2m_o$ is the single-photon recoil frequency and $\nu_b = m_o g/\hbar k$ is the Bloch oscillation frequency.

As for the light field modes, using the Heisenberg equation and adding decay rates for the cavity κ and pump rates $\eta_\pm$, we get

$$\dot{\alpha_\pm} = (i\Delta_c - \kappa)\alpha_\pm + ig_{21}\sum_n c_{1,n\mp1}^* c_{2,n} + \eta_\pm, \quad (6.2.2)$$

where the atoms number can be recovered from the complex amplitudes from the normalization condition (6.1.6). The atomic movement can be described by the momentum operator expectation value:

$$p = \hbar k \sum_n n\Big(|c_{1,n}|^2 + |c_{2,n}|^2\Big), \quad (6.2.3)$$

whose derivative, corresponding to the dipolar force, is given by

$$\dot{p} = i\hbar k g_{21}\sum_n \Big([\alpha_+^* c_{1,n-1}^* c_{2,n} - \alpha_-^* c_{1,n+1}^* c_{2,n}] - c.c.\Big). \quad (6.2.4)$$

We can see in Fig. 22 that the momentum modes populations for the atomic ground states performs the Bloch oscillations due to the optical lattice and external force, and its interaction with the cavity mode α_+ carries information about the atoms motions. The simulation was performed for a constant light field mode $\alpha_- = \eta_-/\kappa$.

However, for low values of detuning for transition $|1\rangle$-$|2\rangle$ the excited level starts to influence on the Bloch oscillations, see Fig. 23. The pulses from the light field mode are damped due to the decoherence in the ground state population $\sum_n |c_{1n}|^2$. Due to the large number of momentum states involved, numerical solutions become very complex and time-consuming when considering the case of a light field far detuned from the atomic resonance ($\Delta_{21} \gg g_{21}$), since one has to deal with many fast oscillations between the atomic level states. To tackle this issue, we can perform an adiabatic elimination of the excited state. When the light fields are very detuned from atomic resonances, the internal and external dynamics occur at very different time scales, where the former varies faster and adapt very rapidly to the boundary conditions defined by the external state and the

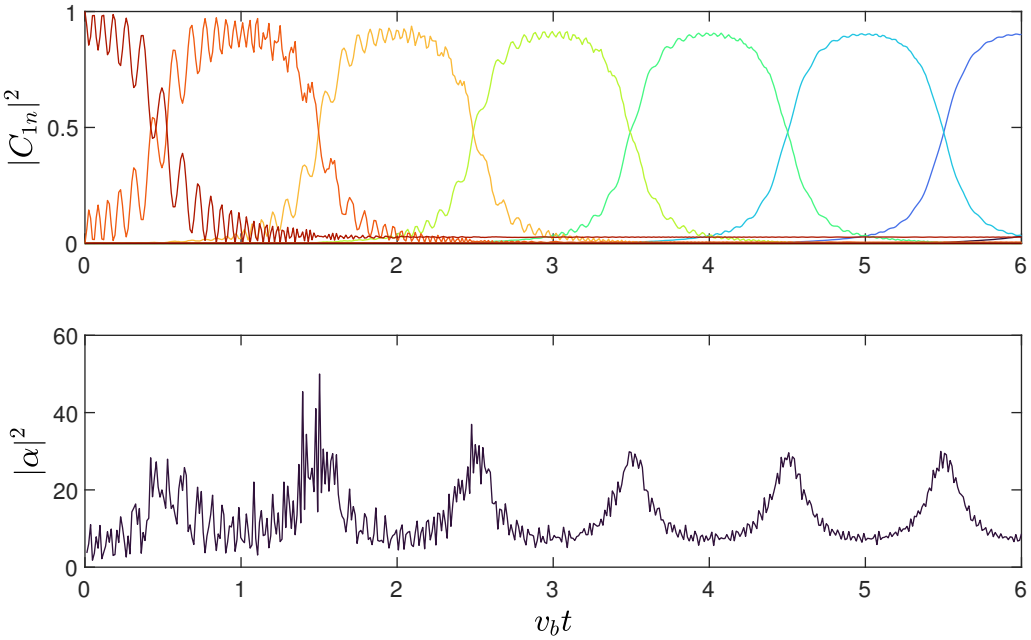

Figure 22 – Time evolution of (top) the momentum modes populations of the atomic ground state, where each color correspond to a momentum mode of even n, and (bottom) the light field mode α_+ intensity. Parameters used for the simulation: $g_{21} = 0.1\omega_r$, $\alpha_- = 1.25$, $\Delta_{21} = 400\omega_r$, $\Delta_c = 0$, $\kappa = 160\omega_r$ and $\nu_b = 0.035\omega_r$ with $N = 4.10^4$ atoms.
Source: By the author.

light field. Therefore, the internal state has no dynamics on the time-scale of the atom motion, and we can adiabatically eliminate the internal degrees of freedom related to the atomic energy levels. Then the coherence between levels transition σ_{21} and populations difference $\mathcal{D}$ reaches the steady-states solutions as derived in section 3.4. Considering the case without spontaneous emissions the solution for the coherence is given by

$$\hat{\sigma}_{21}(\infty) = \frac{i}{2}\frac{\Omega_{21}\Delta_{21}}{|\Omega_{21}|^2 + 2\Delta_{21}^2} \approx \frac{i}{2}\frac{g_{21}(\hat{a}_+ e^{ik\hat{z}} + \hat{a}_- e^{-ik\hat{z}})}{\Delta_{21}}, \tag{6.2.5}$$

where the approximation is performed in the regime where $\Delta_{21}^2 \gg |\Omega_{21}|^2$. Inserting the above equation in equations (6.1.1), we obtain the Hamiltonian for the adiabatic elimination of the excited state without pump

$$\mathcal{H} = \tilde{\mathcal{H}}_{atom} - \frac{i\hbar g_{21}^2}{\Delta_{21}}\left(\hat{a}_+^\dagger e^{-ik_1\hat{z}} + \hat{a}_-^\dagger e^{ik_1\hat{z}}\right)(\hat{a}_+ e^{ik\hat{z}} + \hat{a}_- e^{-ik\hat{z}}) + \hbar\Delta_c \hat{a}_\pm^\dagger \hat{a}_\pm + \frac{\hbar W_o}{2}\sin(2k\hat{z}), \tag{6.2.6}$$

$$\mathcal{H} = \tilde{\mathcal{H}}_{atom} - i\hbar U_o\left(\hat{a}_+^\dagger \hat{a}_- e^{-2ik_1\hat{z}} + \hat{a}_-^\dagger \hat{a}_+ e^{2ik_1\hat{z}}\right) + \hbar(Uo - \Delta_c)\hat{a}_\pm^\dagger \hat{a}_\pm + \frac{\hbar W_o}{2}\sin(2k\hat{z}), \tag{6.2.7}$$

where $U_o = g_{21}^2/\Delta_{21}$ is the pump-probe coupling strength.

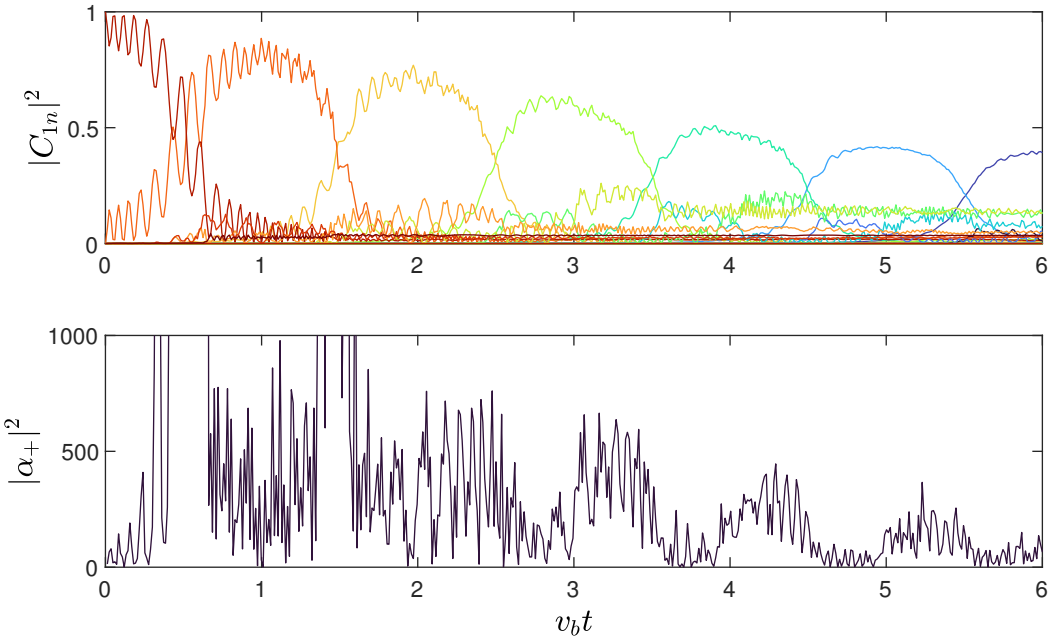

Figure 23 – Time evolution of (top) the momentum modes populations of the atomic ground state, and (bottom) the light field mode α_+ intensity. Parameters used for the simulation are: $g_{21} = 0.1\omega_r$, $\alpha_- = 0.125$, $\Delta_{21} = 200\omega_r$, $\Delta_c = 0$, $\kappa = 160\omega_r$ and $\nu_b = 0.035\omega_r$ with $N = 4.10^4$ atoms.
Source: By the author.

The Hamiltonian eigenstates (6.1.5) consists now only of the momentum states

$$|\Psi(t)\rangle = \sum_n c_n |n\rangle , \tag{6.2.8}$$

and its complex amplitudes derivatives, considering the external force and optical lattice, are given by

$$\frac{\mathrm{d}c_n}{\mathrm{d}t} = i\omega_r(n + 2\nu_b t)^2 c_n + U_o(\tilde{\alpha}^* c_{n+2} + \tilde{\alpha} c_{n-2}), \tag{6.2.9}$$

where $\tilde{\alpha} = \alpha + \alpha_o$ with $\alpha = \left\langle \hat{a}_-^\dagger \hat{a}_+ \right\rangle$ and $\alpha_o = W_o/4U_o$. The light field mode derivative, for a constant probe mode $\dot{\alpha}_- = 0$ can be written as

$$\frac{\mathrm{d}\tilde{\alpha}}{\mathrm{d}t} = U_o \sum_n c_n^* c_{n+2} + (i(U_o + \Delta_c) - \kappa)(\tilde{\alpha} - \alpha_o), \tag{6.2.10}$$

and the average atomic momentum in the accelerated frame is given by

$$\langle \hat{p} \rangle = \sum_n \hbar k n |c_n|^2, \tag{6.2.11}$$

where we can make the transformation $\langle \hat{p} \rangle_{\mathrm{lab}} = \langle \hat{p} \rangle + \nu_b t$ to obtain the momentum in the laboratory frame.

In Fig. 24 we show the system dynamics after the adiabatic elimination of the excited level, where we consider the substitution of $n \to 2n$ in equations (6.2.9) and

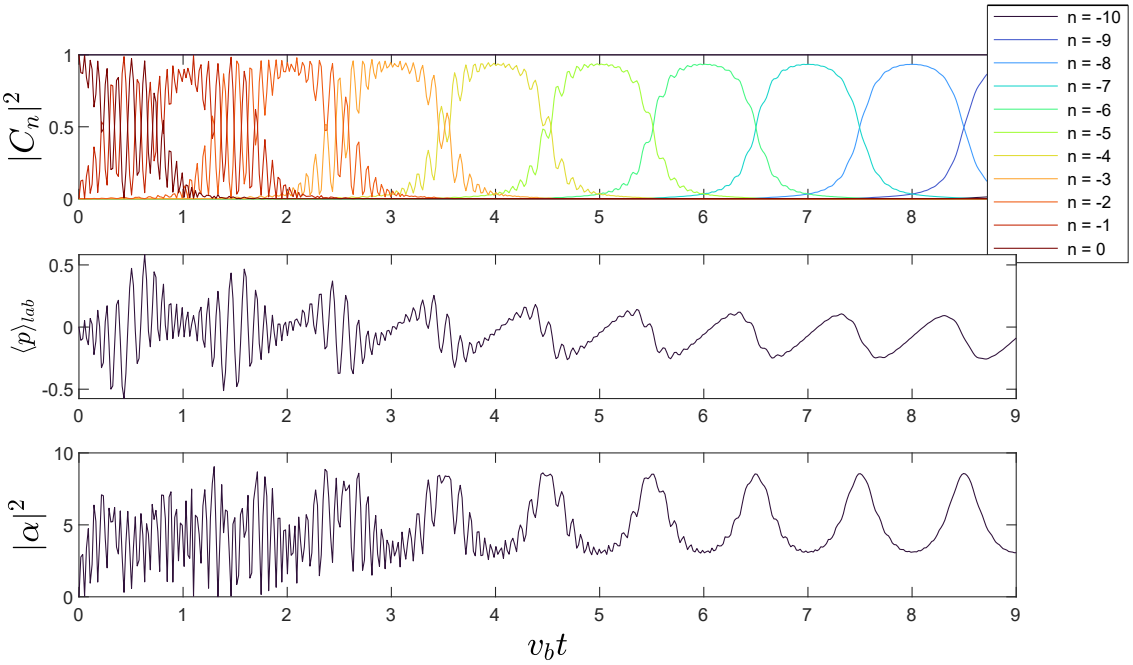

Figure 24 – Time evolution of (top) the momentum modes populations in the adiabatic elimination regime, (middle) the average atomic momentum in the laboratory reference frame with $N = 2.10^4$ atoms and (bottom) the light field mode intensity. Parameters used for the simulation are: $|\alpha_o| = 20$, $\nu_b = 0.035\omega_r$, $U_o = 0.04\omega_r$, $\Delta_c = 0$ and $\kappa = 160\omega_r$.
Source: By the author.

(6.2.10), since the dynamics occurs only at even numbers of n. Neglecting the oscillations between atomic level states allows us to observe more momentum modes oscillations with a reduced integration time of the numerical routine.

In fact we are able to observe the CARL dynamics dominating the system for a large atoms number in Fig. 25, and for a large cooperative coupling NU_o/κ, which manifests as pulses of backscattered photons in the mode α and the acceleration in the average atomic momentum. This can be explained as a scattering of photons from the pumped cavity mode into the reverse mode α, which influence the atoms dynamics. In this regime, the momentum transfer from the fields to the atoms results in the backscattering of the pump light by a self-generated atomic density grating. As a consequence, the population transfer between adjacent momentum states does not occur at the regular Bloch periods ν_b.[8,9]

However, such behavior can not be reproduced by solving equations (6.2.1), since it would require a large detuning to maintain the atoms in the ground state, which in turn is very costly from a numerical standpoint.

6.3 Master equation for the three-level atoms

Let us now derive complete equations from the three-level system. We start by defining the system density matrix regarding the internal and external atomic degrees

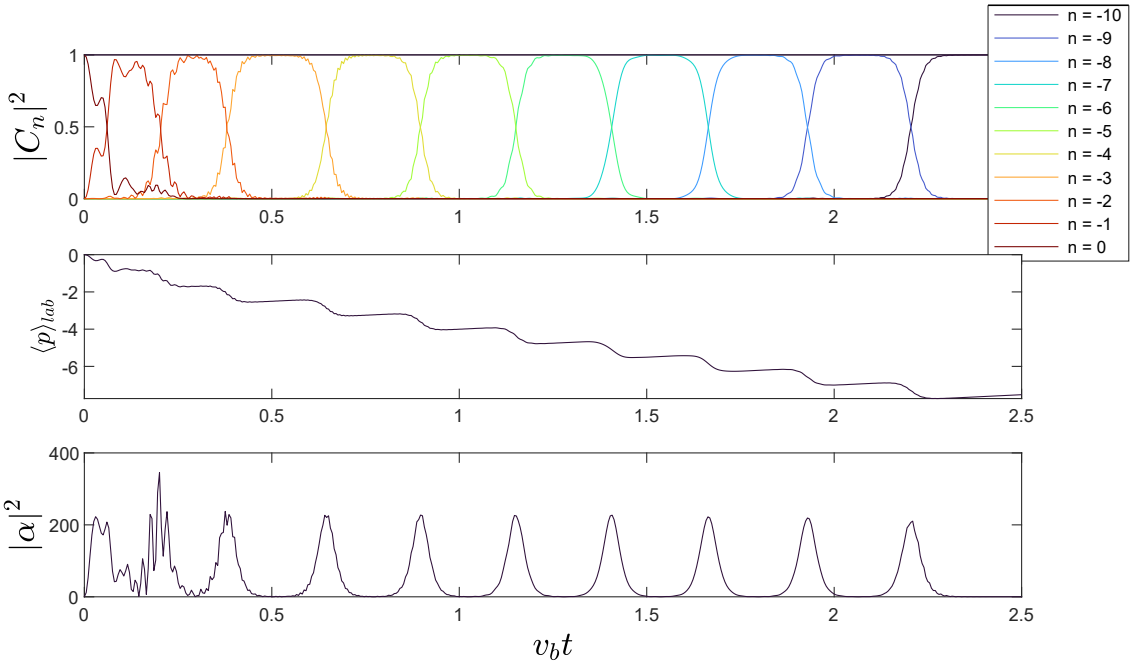

Figure 25 – Time evolution of (top) the momentum modes populations, (middle) the average atomic momentum in the laboratory reference frame with $N = 12.10^4$ atoms and (bottom) the light field mode intensity for the system dominated by CARL dynamics. Parameters used for the simulation are similar to Fig. 24
Source: By the author.

of freedom. To simplify our equations we consider that both light fields have similar wave-numbers $k_1 \approx k_3 \approx k$.

Within the rotating wave approximation we can write the density matrix for the atomic system

$$\hat{\rho}(t) = |\Psi(t)\rangle\langle\Psi(t)|\,, \tag{6.3.1}$$

$$\rho_{ij}^{m,n} = \langle i,m|\,\hat{\rho}\,|j,n\rangle\,. \tag{6.3.2}$$

The equations of motion for the density matrix element is given by the von Neumann equation with the Hamiltonian (6.1.1) and the dissipative term of the Lindblad super-operators:

$$\frac{\mathrm{d}\hat{\rho}}{\mathrm{d}t} = \frac{i}{\hbar}[\hat{\rho},\mathcal{H}] + \mathcal{L}_{atom}\hat{\rho} + \mathcal{L}_{cavity}\hat{\rho}, \tag{6.3.3}$$

which write

$$\mathcal{L}_{atom}\hat{\rho} = -\sum_{i,j}\gamma_{ij}(\hat{\sigma}_{ji}\hat{\sigma}_{ij}\hat{\rho} - 2\hat{\sigma}_{ij}\hat{\rho}\hat{\sigma}_{ji} + \hat{\rho}\hat{\sigma}_{ji}\hat{\sigma}_{ij}), \tag{6.3.4}$$

$$\mathcal{L}_{cav}\hat{\rho} = -\kappa\Big(\hat{a}_{\pm}^{\dagger}\hat{a}_{\pm}\hat{\rho} - 2\hat{a}_{\pm}\hat{\rho}\hat{a}_{\pm}^{\dagger} + \hat{\rho}\hat{a}_{\pm}^{\dagger}\hat{a}_{\pm}\Big). \tag{6.3.5}$$

Then, the derivative of each density matrix element is written as

$$\dot{\rho}_{ij}^{m,n} = \frac{i}{\hbar}\langle i,m|\,[\hat{\rho},\mathcal{H}_{atom}+\mathcal{H}_{int}]\,|j,n\rangle + \langle i,m|\,\mathcal{L}_{atom}\hat{\rho}\,|j,n\rangle\,. \tag{6.3.6}$$

Expanding the first term in the RHS of the above expression (denominated the coherent part), we obtain

$$\langle i,m|\,[\hat{\rho},\mathcal{H}_{at,int}]\,|j,n\rangle = \langle i,m|\,\hat{\rho}\sum_{v,q}|v,q\rangle\langle v,q|\,\mathcal{H}_{at,int}\,|j,n\rangle - \langle i,m|\,\mathcal{H}_{at,int}\sum_{u,p}|u,p\rangle\langle u,p|\,\hat{\rho}\,|j,n\rangle\,, \quad (6.3.7)$$

$$\langle i,m|\,[\hat{\rho},\mathcal{H}_{at,int}]\,|j,n\rangle = \sum_{v,q}\rho_{i,v}^{m,q}\,\langle v,q|\,\mathcal{H}_{at,int}\,|j,n\rangle - \sum_{u,p}\langle i,m|\,\mathcal{H}_{at,int}\,|u,p\rangle\,\rho_{u,j}^{p,n}, \quad (6.3.8)$$

$$\begin{aligned}\langle i,m|\,[\mathcal{H}_{at,int},\hat{\rho}]\,|j,n\rangle = \hbar\left[\frac{(n^2-m^2)\hbar k^2}{2m_o} - \Delta_{21}(\delta_{j2}-\delta_{i2}) - \Delta_{32}(\delta_{j3}-\delta_{i3})\right]\rho_{ij}^{m,n}\\ - \hbar g_{21}\Big[\alpha_+^*\Big(\delta_{i1}\rho_{2j}^{m+1,n} - \delta_{j2}\rho_{i1}^{m,n-1}\Big) + \alpha_-^*\Big(\delta_{i1}\rho_{2j}^{m-1,n} - \delta_{j2}\rho_{i1}^{m,n+1}\Big)\Big]\\ - \hbar g_{21}\Big[\alpha_+\Big(\delta_{i2}\rho_{1j}^{m-1,n} - \delta_{j1}\rho_{i2}^{m,n+1}\Big) + \alpha_-\Big(\delta_{i2}\rho_{1j}^{m+1,n} - \delta_{j1}\rho_{i2}^{m,n-1}\Big)\Big]\\ - \hbar g_{32}\alpha_3^*\Big(\delta_{i2}\rho_{3j}^{m+1,n} - \delta_{j3}\rho_{i2}^{m,n-1}\Big) - \hbar g_{32}\alpha_3\Big(\delta_{i3}\rho_{2j}^{m-1,n} - \delta_{j2}\rho_{i3}^{m,n+1}\Big). \quad (6.3.9)\end{aligned}$$

As for the incoherent part of equation (6.3.6), one gets

$$\langle i,m|\,\mathcal{L}_{atom}\hat{\rho}\,|j,n\rangle = -\sum_{k,l}\langle i,m|\,\gamma_{kl}(\hat{\sigma}_{lk}\hat{\sigma}_{kl}\hat{\rho} - 2\hat{\sigma}_{kl}\hat{\rho}\hat{\sigma}_{lk} + \hat{\rho}\hat{\sigma}_{lk}\hat{\sigma}_{kl})\,|j,n\rangle\,, \quad (6.3.10)$$

$$\begin{aligned}\langle i,m|\,\mathcal{L}_{atom}\hat{\rho}\,|j,n\rangle = -\sum_{k,l}\langle i,m|\,\gamma_{kl}\hat{\sigma}_{lk}\hat{\sigma}_{kl}\sum_{u,p}|u,p\rangle\langle u,p|\,\hat{\rho}\,|j,n\rangle\\ + 2\sum_{k,l}\gamma_{kl}\,\langle i,m|\,\hat{\sigma}_{kl}\sum_{u,p}|u,p\rangle\langle u,p|\,\hat{\rho}\sum_{v,q}|v,q\rangle\langle v,q|\,\hat{\sigma}_{lk}\,|j,n\rangle\\ - \sum_{k,l}\gamma_{kl}\,\langle i,m|\,\hat{\rho}\sum_{u,p}|u,p\rangle\langle u,p|\,\hat{\sigma}_{lk}\hat{\sigma}_{kl}\,|j,n\rangle\,, \quad (6.3.11)\end{aligned}$$

$$\begin{aligned}\langle i,m|\,\mathcal{L}_{atom}\hat{\rho}\,|j,n\rangle = \sum_{k,l}\sum_{u,p,q,v}2\gamma_{kl}\,\langle i,m|\,\hat{\sigma}_{kl}\,|u,p\rangle\,\rho_{u,v}^{p,q}\,\langle v,q|\,\hat{\sigma}_{lk}\,|j,n\rangle\\ - \sum_{k,l,u,p}\gamma_{kl}\,\langle i,m|\,\hat{\sigma}_{lk}\hat{\sigma}_{kl}\,|u,p\rangle\,\rho_{u,j}^{p,n} - \sum_{k,l,u,p}\gamma_{kl}\rho_{i,u}^{m,p}\,\langle u,p|\,\hat{\sigma}_{lk}\hat{\sigma}_{kl}\,|j,n\rangle\,, \quad (6.3.12)\end{aligned}$$

$$\langle i,m|\,\mathcal{L}_{atom}\hat{\rho}\,|j,n\rangle = \sum_{k,l}2\delta_{i,k}\delta_{jk}\gamma_{kl}\rho_{l,l}^{m,n} - \sum_{k}(\gamma_{ki}+\gamma_{kj})\rho_{ij}^{m,n}. \quad (6.3.13)$$

Gathering all the equations we obtain from the following derivative for the density matrix elements

$$\begin{aligned}\dot{\rho}_{ij}^{m,n} = i\left[\frac{\hbar k^2}{2m_o}(n^2-m^2) - \Delta_{21}(\delta_{j2}-\delta_{i2}) - \Delta_{32}(\delta_{j3}-\delta_{i3})\right]\rho_{ij}^{m,n}\\ - ig_{21}\Big[\alpha_+^*\Big(\delta_{i1}\rho_{2j}^{m+1,n} - \delta_{j2}\rho_{i1}^{m,n-1}\Big) + \alpha_-^*\Big(\delta_{i1}\rho_{2j}^{m-1,n} - \delta_{j2}\rho_{i1}^{m,n+1}\Big)\Big]\\ - ig_{21}\Big[\alpha_+\Big(\delta_{i2}\rho_{1j}^{m-1,n} - \delta_{j1}\rho_{i2}^{m,n+1}\Big) + \alpha_-\Big(\delta_{i2}\rho_{1j}^{m+1,n} - \delta_{j1}\rho_{i2}^{m,n-1}\Big)\Big]\\ - ig_{32}\alpha_3^*\Big(\delta_{i2}\rho_{3j}^{m+1,n} - \delta_{j3}\rho_{i2}^{m,n-1}\Big) - ig_{32}\alpha_3\Big(\delta_{i3}\rho_{2j}^{m-1,n} - \delta_{j2}\rho_{i3}^{m,n+1}\Big)\\ + \sum_{k,l}2\delta_{i,k}\delta_{jk}\gamma_{kl}\rho_{l,l}^{m,n} - \sum_{k}(\gamma_{ki}+\gamma_{kj})\rho_{ij}^{m,n}. \quad (6.3.14)\end{aligned}$$

The derivatives for each element of the density matrix, after performing the transformation into the driving fields frame 3.2.1, read

$$\begin{aligned}\dot{\rho}_{11}^{m,n} &= i\omega_r^{mn}\rho_{11}^{m,n} + \Gamma_{12}\rho_{22}^{m,n} + \Gamma_{13}\rho_{33}^{m,n} \\ &\quad - ig_{21}\Big(\alpha_+^*\sigma_{21}^{m+1,n} + \alpha_-^*\sigma_{21}^{m-1,n} - \alpha_+\sigma_{12}^{m,n+1} - \alpha_-\sigma_{12}^{m,n-1}\Big),\end{aligned} \tag{6.3.15a}$$

$$\begin{aligned}\dot{\rho}_{22}^{m,n} &= i\omega_r^{mn}\rho_{22}^{m,n} - \Gamma_{12}\rho_{22}^{m,n} + \Gamma_{23}\rho_{33}^{m,n} - ig_{32}\Big(\alpha_3^*\sigma_{32}^{m+1,n} - \alpha_3\sigma_{23}^{m,n+1}\Big) \\ &\quad + ig_{21}\Big(\alpha_+^*\sigma_{21}^{m,n-1} + \alpha_-^*\sigma_{21}^{m,n+1} - \alpha_+\sigma_{12}^{m-1,n} - \alpha_-\sigma_{12}^{m+1,n}\Big),\end{aligned} \tag{6.3.15b}$$

$$\dot{\rho}_{33}^{m,n} = i\omega_r^{mn}\rho_{33}^{m,n} - (\Gamma_{23}+\Gamma_{13})\rho_{33}^{m,n} + ig_{32}\Big(\alpha_3^*\sigma_{32}^{m,n-1} - \alpha_3\sigma_{23}^{m-1,n}\Big), \tag{6.3.15c}$$

$$\begin{aligned}\dot{\sigma}_{21}^{m,n} &= -\left(\frac{\Gamma_{12}}{2} - i\Delta_{21}^{mn}\right)\sigma_{21}^{m,n} + ig_{32}\alpha_3^*\sigma_{31}^{m+1,n} \\ &\quad - ig_{21}\Big[\alpha_+\Big(\rho_{11}^{m-1,n} - \rho_{22}^{m,n+1}\Big) + \alpha_-\Big(\rho_{11}^{m+1,n} - \rho_{22}^{m,n-1}\Big)\Big],\end{aligned} \tag{6.3.15d}$$

$$\dot{\sigma}_{31}^{m,n} = -\left(\frac{\Gamma_{13}}{2} - i\Delta_{31}^{mn}\right)\sigma_{31}^{m,n} + ig_{32}\alpha_3\sigma_{21}^{m-1,n} - ig_{21}\Big(\alpha_+^*\sigma_{32}^{m,n+1} + \alpha_-^*\sigma_{32}^{m,n-1}\Big), \tag{6.3.15e}$$

$$\dot{\sigma}_{32}^{m,n} = -\left(\frac{\Gamma_{23}}{2} - i\Delta_{32}^{mn}\right)\sigma_{32}^{m,n} + ig_{21}\Big(\alpha_+^*\sigma_{31}^{m,n-1} + \alpha_-^*\sigma_{31}^{m,n+1}\Big) - ig_{32}\alpha_3\Big(\rho_{22}^{m-1,n} - \rho_{33}^{m,n+1}\Big), \tag{6.3.15f}$$

where $\rho_{ij} = \sigma_{ij}e^{i\tilde{\omega}}$, $\Delta_{ij}^{mn} = \omega_{ij} + \omega_r^{mn} - \tilde{\omega}$, $\omega_r^{nm} = (n^2 - m^2)\frac{\hbar k^2}{2m_o}$ is the recoil frequency for a momentum transition from n to m and $\Gamma_{ij} = 2\gamma_{ij}$ the linewidth of the respective atomic level transition. The phases $e^{i\tilde{\omega}t}$ are absorbed by the fields amplitudes α.

From the Heisenberg equation the fields equations of motion yields

$$\dot{\alpha}_+ = (i\Delta_c - \kappa)\alpha_+ - ig_{21}\sum_n \sigma_{12}^{n-1,n} + \eta_+, \tag{6.3.16a}$$

$$\dot{\alpha}_- = (i\Delta_c - \kappa)\alpha_- - ig_{21}\sum_n \sigma_{12}^{n+1,n} + \eta_-. \tag{6.3.16b}$$

The derivative for the density matrix element with the external force includes the term $-\frac{2i\hbar k^2}{m_o}(m-n)\nu_b t\rho_{ij}^{m,n}$ in 6.3.14, where $\nu_b = m_o a/2\hbar k$. In order to avoid repeating the equations (6.3.15) we can include this term into the recoil frequency as

$$\omega_r^{m,n} = \frac{\hbar k^2}{2m_o}\Big[(n^2 - m^2) + 4(n-m)\nu_b t\Big]. \tag{6.3.17}$$

The corresponding terms in the density matrix elements derivatives from the optical lattice are given by the Hamiltonian in equation (6.1.7)

$$\frac{i}{\hbar}[\hat{\rho}, \mathcal{H}_{latt}] = -\frac{W_o}{4}\Big[\Big(e^{2ikz} - e^{-2ikz}\Big), \hat{\rho}\Big], \tag{6.3.18}$$

$$\langle i, m|\left[e^{\pm 2ikz}, \hat{\rho}\right]|j, n\rangle = \rho_{ij}^{m\mp 2,n} - \rho_{ij}^{m,n\pm 2}, \tag{6.3.19}$$

which can be added to equations (6.3.14) as

$$-\frac{W_o}{4}\Big(\rho_{ij}^{m-2,n} - \rho_{ij}^{m,n+2} - \rho_{ij}^{m+2,n} + \rho_{ij}^{m,n-2}\Big). \tag{6.3.20}$$

6.4 Results

In this section we present the obtained results for equations (6.3.15) in presence of the gravity and optical lattice. At first, we reproduce the dynamics for the 2LA as shown by Fig. 26, where the third level is "turned off" by setting $g_{32} = 0$.

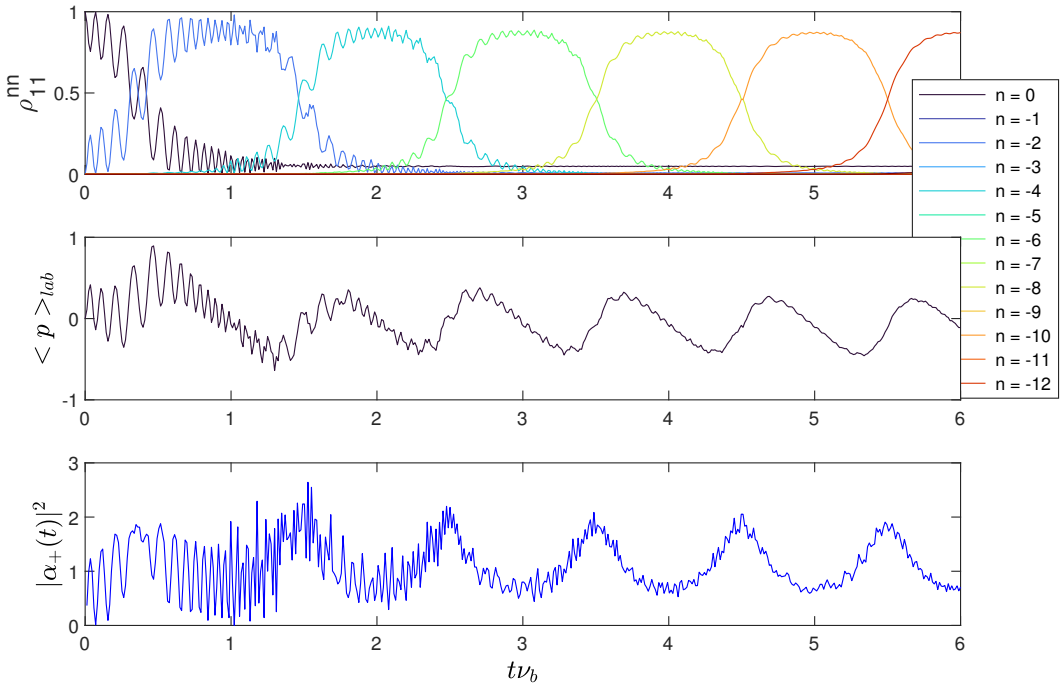

Figure 26 – (top) Bloch oscillations for a two-level atom by solving equations (6.3.15) with $g_{32} = 0$, (middle) average atomic momentum in the laboratory reference frame (in $\hbar k$) with $N = 4.10^4$ atoms and (bottom) time evolution of the light field mode intensity. Parameters used for the simulation are: $\alpha_- = 10^2$, $\nu_b = 0.035\omega_r$, $U_o = 0.04\omega_r$, $\Delta_c = 0$, $\kappa = 160\omega_r$, $\Delta_{21} = 50\omega_r$ and $g_{21} = 0.1\omega_r$. Source: By the author.

The main interest of solving the master equation for this system is to include the dissipation effect of the spontaneous emission. In Fig. 27 we can observe this effect on the Bloch oscillations for a large detuning $\Delta_{21} = 2.10^3\Gamma_{21}$. The decoherence on the atoms dynamics occurs as odd momentum modes of the ground state are populated (dashed lines in the figures). Those momentum modes come from the excited state, which decays according to the term $\Gamma_{21}\rho_{22}^{m,n}$ in equation (6.3.15b).

For the dynamics, it is required to include positive momentum modes in the numerical routine. A full spectrum of n would show that those momentum modes are also populated throughout the system dynamic, but this effect is rather weak, as can be summarized in the mode $n = 2$, see Fig. 27 and 28.[26] The atoms in those modes are eliminated from the cloud since they are accelerated towards gravity, and their influence on the light fields are negligible for small decay rates.

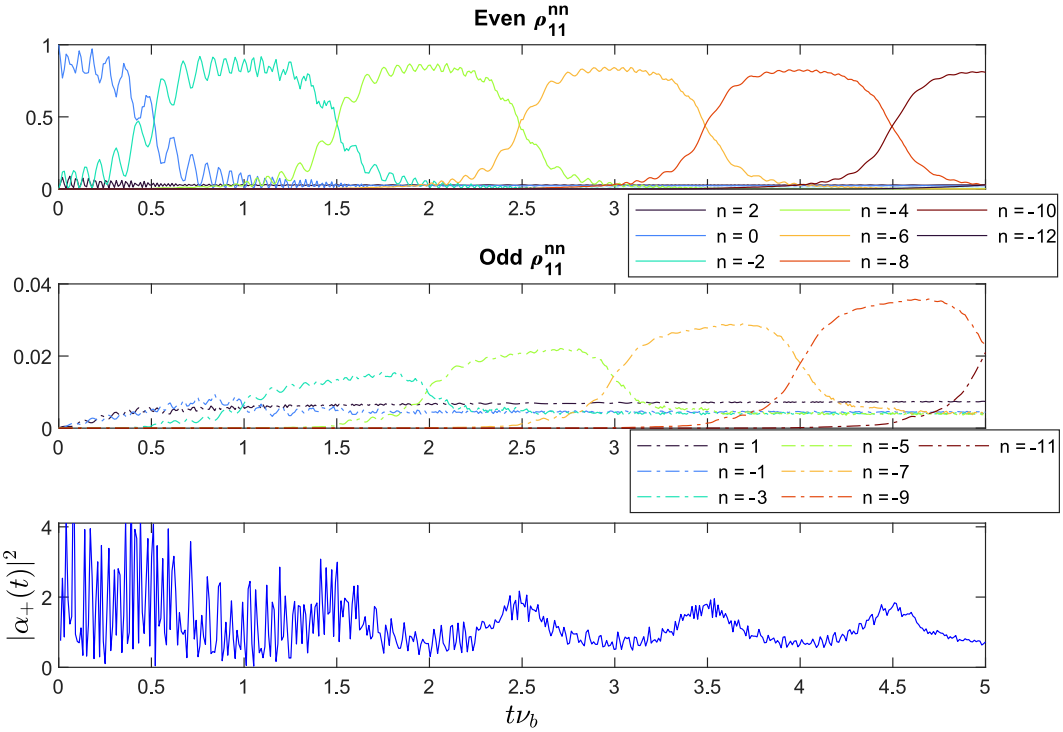

Figure 27 – Dissipation effect on the Bloch oscillations for a decay rate of $\Gamma_{21} = .05\omega_r$, $\Delta_{21} = 100\omega_r$, $g_{21} = 0.1\omega_r$ and $\alpha_- = 10^2$.
Source: By the author.

Although the odd momentum modes overcome the even modes, for higher decay rates we can note that actually more atoms are expelled from the cloud as the even and odd modes decrease, see Fig. 28. With fewer atoms performing the Bloch oscillations, the oscillations signals on the light field mode α_+ decays rapidly.

Turning on the third level we can observe momentum modes oscillations in each level, see Fig. 29, which depicts a non-dissipative three-level system. The growth of the excited levels momentum modes is a probable signature of the CARL phenomenon, which increases the excited atoms momentum, accelerating their average momentum upwards the gravity.

Adding the spontaneous emission to the three-level atom dynamics, in Fig. 31 we can see the growth of the odd momentum modes of the ground state, while the excited states reaches stationary values. Comparing to the two-level case in Fig. 30, there is a substantial reduction on the odd modes. Regarding the results in Chapter 5, unfortunately to reach the region of EIT it would require a much higher light-atom coupling force g_{32} for the transition $|2\rangle$-$|3\rangle$ to efficiently eliminate the system dissipation.

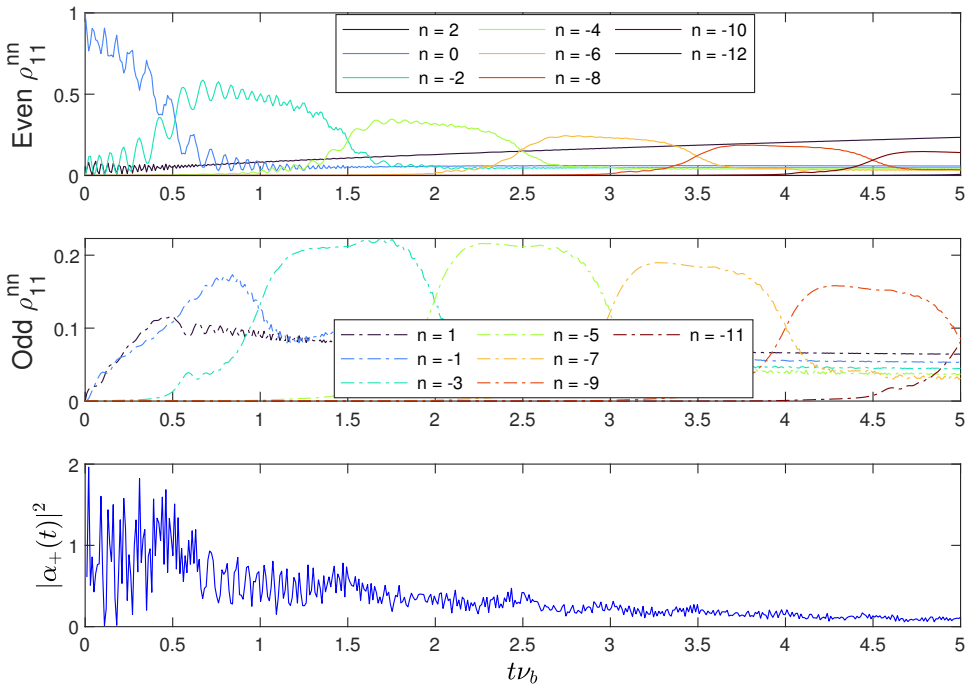

Figure 28 – Dissipation effect on the Bloch oscillations for a decay rate of $\Gamma_{21} = 2.5\omega_r$, $\Delta_{21} = 100\omega_r$, $g_{21} = 0.1\omega_r$ and $\alpha_- = 10^2$.
Source: By the author.

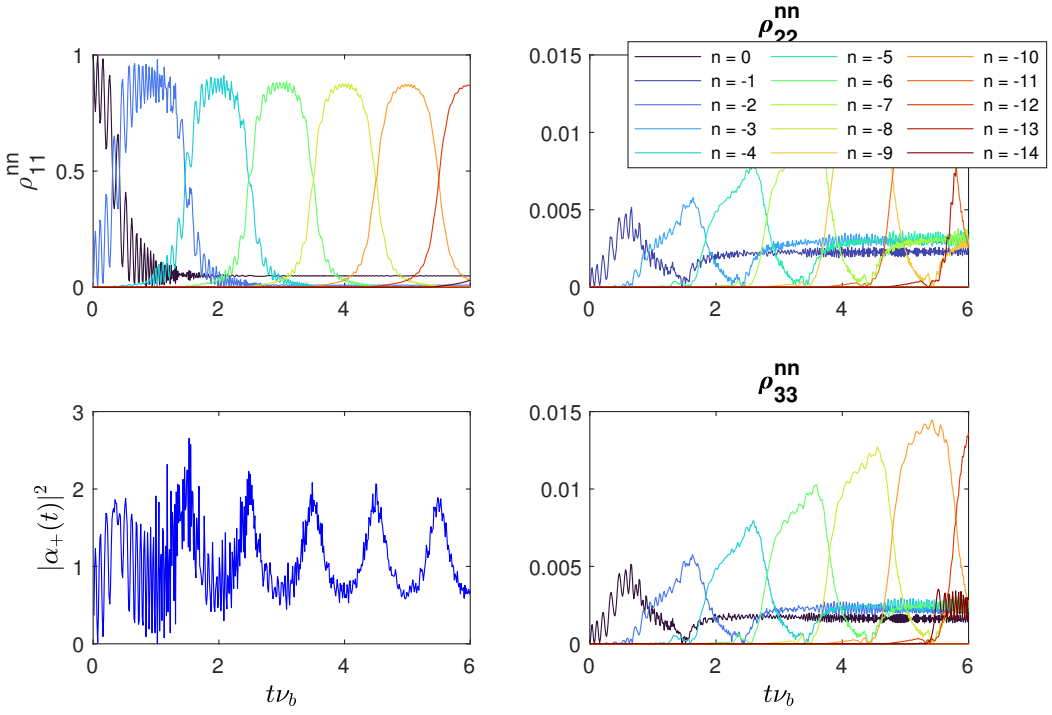

Figure 29 – Bloch oscillations on the three atomic levels without dissipation. Parameters for the figure are: $\Delta_{21} = 50$, $\Gamma_{21} = \Gamma_{32} = 0$, $g_{21} = 0.1\omega_r$ and $g_{32} = 10\omega_r$.
Source: By the author.

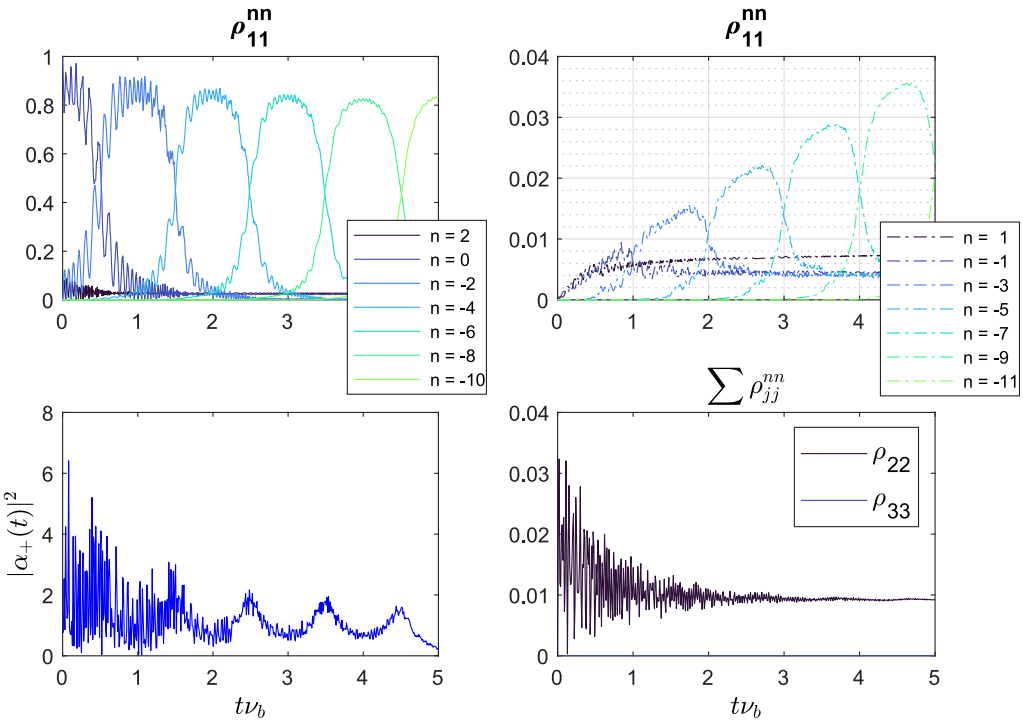

Figure 30 – Bloch oscillations on two atomic levels with dissipation. Parameters for the figure are: $\Delta_{21} = 50$, $\Gamma_{21} = 0.05\omega_r$, $\Gamma_{32} = 0$, $g_{21} = 0.1\omega_r$ and $g_{32} = 0\omega_r$.
Source: By the author.

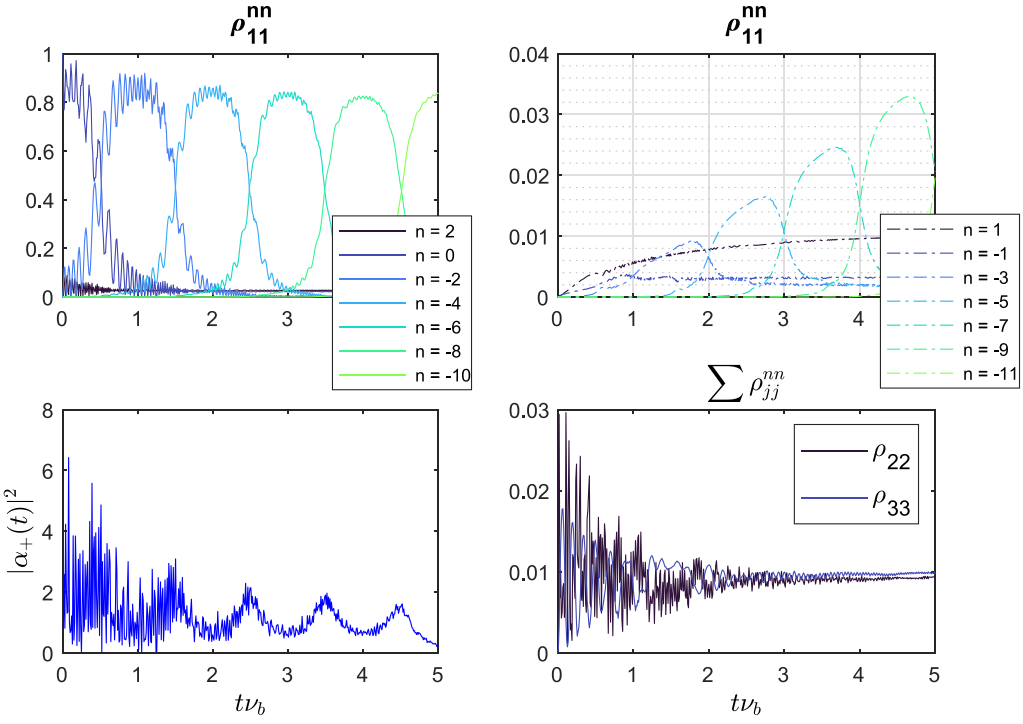

Figure 31 – Bloch oscillations on three atomic levels with dissipation. Parameters for the figure are: $\Delta_{21} = 50$, $\Gamma_{21} = 0.05\omega_r$, $\Gamma_{32} = 0$, $g_{21} = 0.1\omega_r$ and $g_{32} = 10\omega_r$.
Source: By the author.

7 CONCLUSIONS

In the previous chapter, we derived the equations of motion for the three-level atoms system interacting with light fields driving the two transitions. The contributions of an optical lattice and the gravity force were considered, in order to combine the CARL phenomenon and the Bloch oscillations in the system, which required a plane wave expansion of the atoms wave-function. With this, we considered entangled states that combined the atomic momentum mode and its internal energy level. We also considered an approximation assuming the same wave-numbers for the two transitions, so that we could analyse the movement of the atoms in each level with the same plane wave expansion and in the same direction. Other configurations lead to a more complex form for the equations of motion, where a much larger momentum space would be accessible to the atoms.[27]

The set of coupled differential equations for the density matrix elements and for the coupled dynamics of the light field modes allows us to perform numerical routines to simulate the atoms momentum dynamics over several Bloch oscillations. As we do not consider an adiabatic elimination of the excited levels, these equations involve more variables than previous works.[9] Thus, the obtained results are valid for small detuning and light-atom coupling strength. Using the master equation formalism, we were able to analyse the influence of spontaneous emission on the Bloch oscillations. We showed that this dissipation phenomenon suppress the modes oscillations, while populating intermediate modes that did not appear before in the ground state. Although one could expect that those intermediate mode oscillations would remain throughout the dynamics, they saturate and then decay. This decay is accompanied by the atoms stopping to interact with the light, as the population of positive momentum modes (in the gravity reference frame) increases throughout the dynamics.

A possible solution to this problem would be the EIT, whose influence on the dissipative radiative pressure force was analysed in chapter 5. However, to reach the region where this phenomenon is expected to occur, computational resources with higher capacities are required. Here we have presented results showing that even for a region where the radiative pressure is not efficiently suppressed, the dissipation of the momentum modes oscillations is reduced. Those preliminary results motivate us to continue the investigation of Bloch oscillations close to regions where the EIT influence on the system is substantial, with the adoption of more advanced numerical methods. The EIT in the Λ three-level atom configuration is also worth investigating, since our results show that the radiative pressure force reduction relies on a condition between the decay rates of the levels transitions for a cascade configuration, which limits the relevant atomic species.

An effect that can be better investigated is the dynamics considering a full spectrum

of the momentum modes, as in recent works where two matter waves performing Bloch oscillations were combined.[26] This would allow the investigation of matter-wave performing Bloch oscillations in a ring cavity, such that their interaction with the light field leads to an interference, which can carry extra information of the atoms motion.

REFERENCES

1 MARSON, I. A short walk along the gravimeters path. **International Journal of Geophysics**, Hindawi Limited, v. 2012, p. 1–9, 2012. DOI: 10.1155/2012/687813.

2 ROATI, G. *et al.* Atom interferometry with trapped fermi gases. **Physical Review Letters**, American Physical Society (APS), v. 92, n. 23, p. 230402, June 2004.

3 BLOCH, F. Uber die quantenmechanik der elektronen in kristallgittern. **Zeitschrift für Physik**, Springer Science and Business Media LLC, v. 52, n. 7-8, p. 555–600, July 1929.

4 DAHAN, M. B. *et al.* Bloch oscillations of atoms in an optical potential. **Physical Review Letters**, American Physical Society (APS), v. 76, n. 24, p. 4508–4511, June 1996.

5 FERRARI, G. *et al.* Long-lived bloch oscillations with bosonic sr atoms and application to gravity measurement at the micrometer scale. **Physical Review Letters**, American Physical Society (APS), v. 97, n. 6, p. 060402, Aug. 2006.

6 GUSTAVSSON, M. *et al.* Control of interaction-induced dephasing of bloch oscillations. **Physical Review Letters**, American Physical Society (APS), v. 100, n. 8, p. 080404, Feb. 2008.

7 BATTESTI, R. *et al.* Bloch oscillations of ultracold atoms: a tool for a metrological determination of h/m_{rb}. **Physical Review Letters**, American Physical Society, v. 92, p. 253001, June 2004.

8 SAMOYLOVA, M. *et al.* Mode-locked bloch oscillations in a ring cavity. **Laser Physics Letters**, IOP Publishing, v. 11, n. 12, p. 126005, Nov. 2014.

9 SAMOYLOVA, M. *et al.* Synchronization of bloch oscillations by a ring cavity. **Optics Express**, Optical Society of America, v. 23, n. 11, p. 14823, May 2015.

10 SAMOYLOVA, M. **Stabilization of bloch oscillations of ultracold atoms in a ring cavity**. 2015. Tesi (Dottorato) — Università degli Studi di Milano, Milano, 2015.

11 GLUCK, M. *et al.* Calculation of wannier-bloch and wannier-stark states. **The European Physical Journal D**, Springer Science and Business Media LLC, v. 4, n. 3, p. 239–246, Dec. 1998.

12 LARSON, J. Level crossings in a cavity QED model. **Physical Review A**, American Physical Society (APS), v. 73, n. 1, p. 013823, Jan. 2006.

13 MAUNZ, P. *et al.* Cavity cooling of a single atom. **Nature**, Nature Publishing Group, v. 428, n. 6978, p. 50, 2004.

14 COURTEILLE, P. W. The collective atomic recoil laser. **AIP Conference Proceedings**, v. 770, n. 1, p. 135, 2005.

15 KRUSE, D. *et al.* Observation of lasing mediated by collective atomic recoil. **Physical Review Letters**, APS, v. 91, n. 18, p. 183601, 2003.

16 ALLEN, L. **Optical resonance and two-level atoms**. New York: Wiley, 1975. ISBN 0471023272.

17 LOUDON, R. **The quantum theory of light**: Oxford: Oxford University Press, 2000. ISBN 0198501765.

18 GERRY, C.; KNIGHT, P. **Introductory quantum optics**: Cambrigde: Cambridge University Press, 2004.

19 MEYSTRE, P.; SARGENT, M. (ed.). **Elements of quantum optics**. Berlin: Springer Verlag, 2007.

20 MANZANO, D. A short introduction to the lindblad master equation. **AIP Advances**, AIP Publishing, v. 10, n. 2, p. 025106, Feb. 2020.

21 HARRIS, S. E. Electromagnetically induced transparency. **Physics Today**, AIP Publishing, v. 50, n. 7, p. 36–42, July 1997.

22 FLEISCHHAUER, M.; IMAMOGLU, A.; MARANGOS, J. P. Electromagnetically induced transparency: optics in coherent media. **Reviews of Modern Physics**, American Physical Society (APS), v. 77, n. 2, p. 633–673, July 2005.

23 MARANGOS, J. P. Electromagnetically induced transparency. **Journal of Modern Optics**, Taylor & Francis, v. 45, n. 3, p. 471–503, Mar. 1998.

24 HARRIS, S. E.; FIELD, J. E.; IMAMOGLU, A. Nonlinear optical processes using electromagnetically induced transparency. **Physical Review Letters**, American Physical Society, v. 64, n. 10, p. 1107–1110, Mar. 1990.

25 ABI-SALLOUM, T. Y. Eit and at: two similar but distinct phenomena in two categories of three-level atomic systems. **Physical Review A**, American Physical Society (APS), v. 81, n. 5, p. 053836, May 2010.

26 PAGEL, Z. *et al.* Symmetric bloch oscillations of matter waves. **Physical Review A**, American Physical Society (APS), v. 102, n. 5, p. 053312, Nov. 2020.

27 BUX, S. *et al.* Control of matter-wave superradiance with a high-finesse ring cavity. **Physical Review A**, American Physical Society (APS), v. 87, n. 2, p. 023607, Feb. 2013.